Gas hydrate evaluation / Cyclostratigraphy
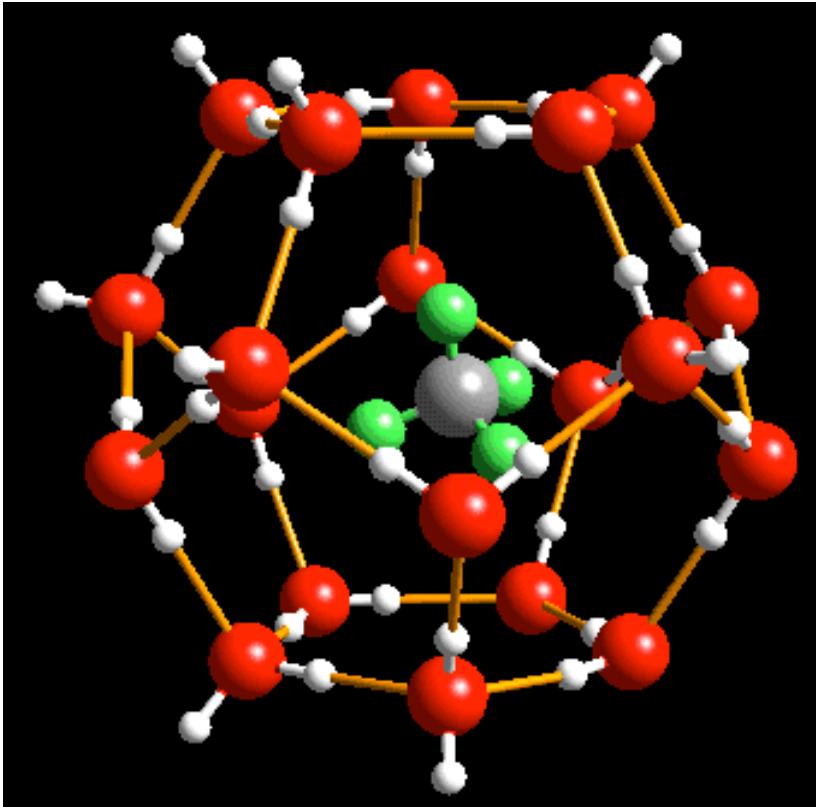
Alberto Malinverno

Well Logging Principles and Applications
G9947 - Seminar in Marine Geophysics
Spring 2008

Outline

- Introduction to gas hydrates
- Estimating gas hydrate abundance with downhole logs
  - Electrical resistivity
  - Acoustic
  - Nuclear magnetic resonance (NMR)
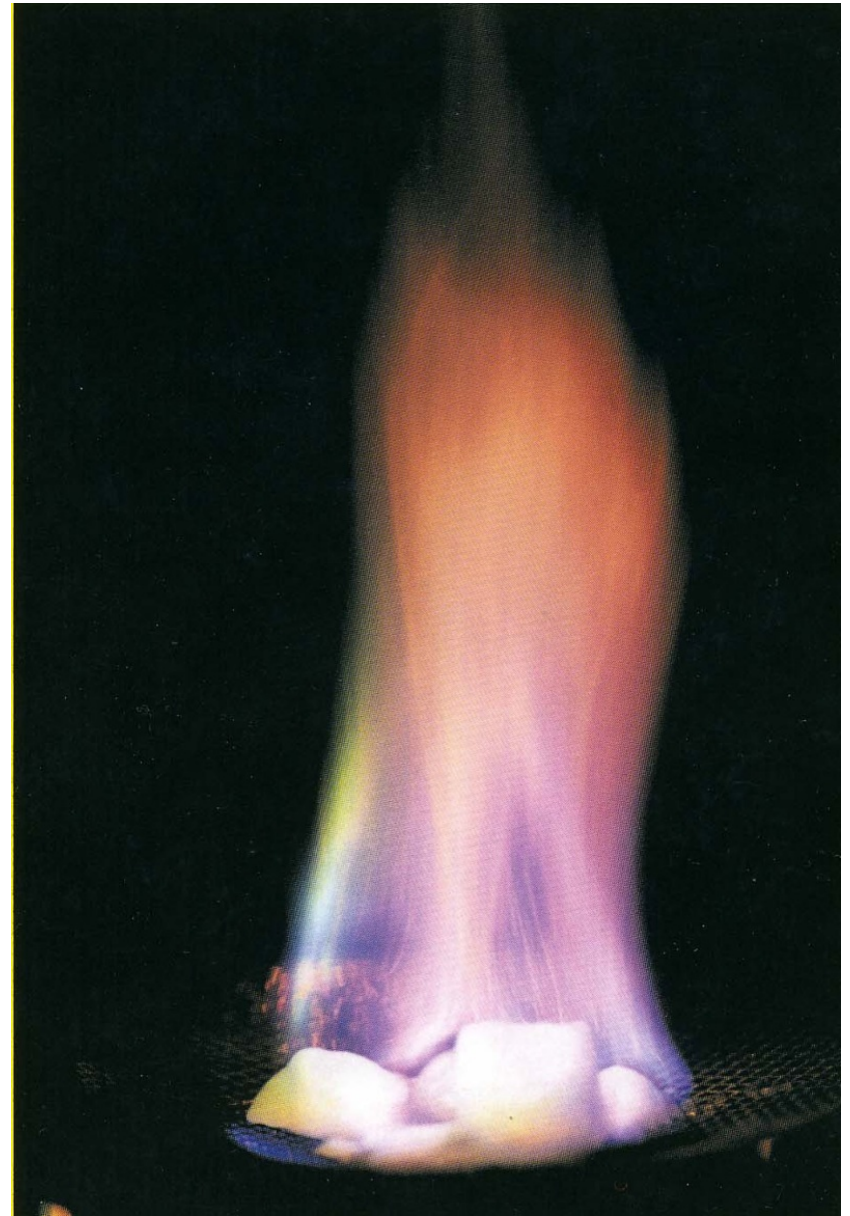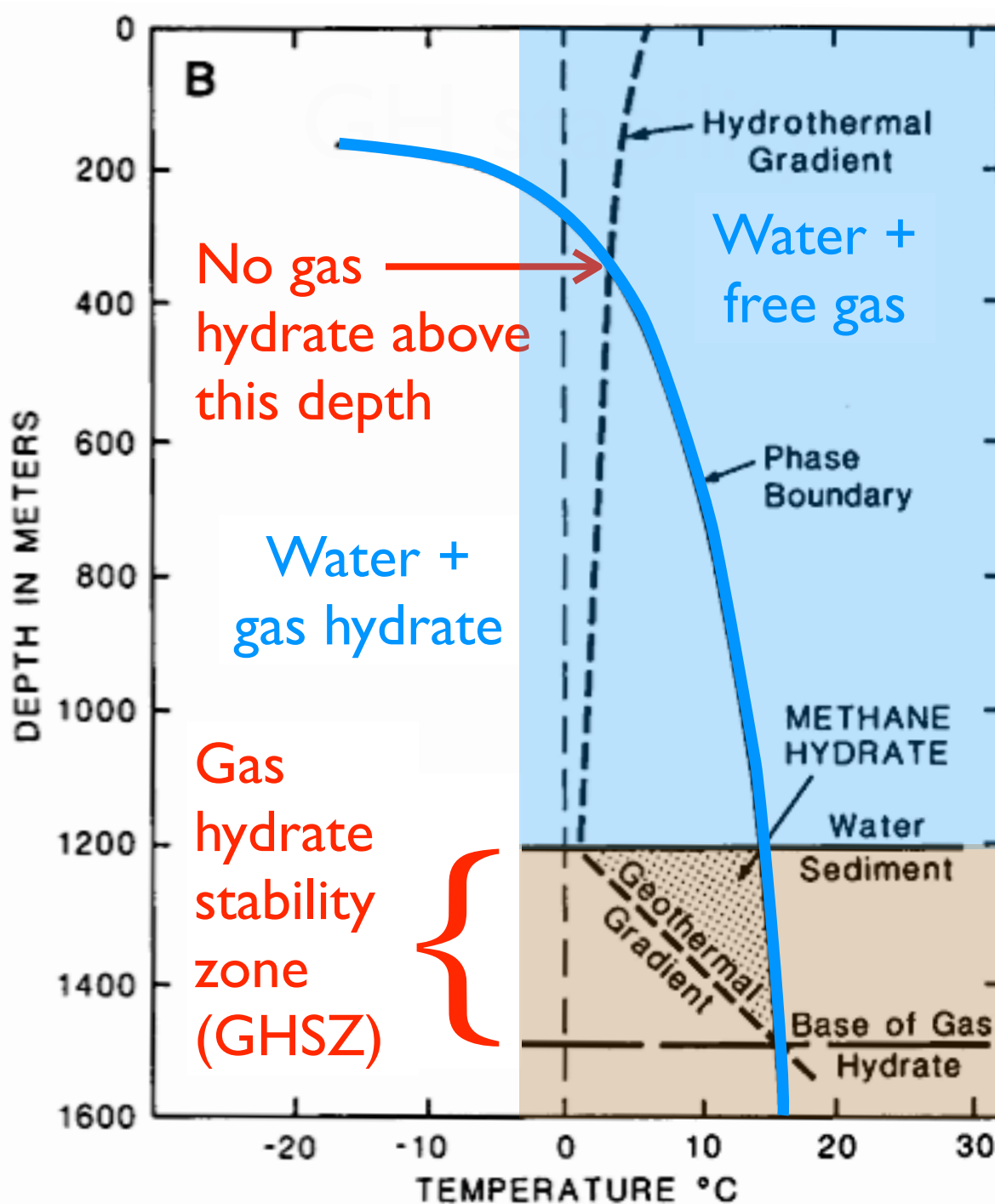- Cyclostratigraphy with downhole logs

Fire and ice

Clathrate
(Chemistry) a compound in which molecules of one component are physically trapped within the crystal structure of another. ORIGIN 1940s: from L. clathratus, from clathri 'lattice-bars'.

B

DEPTH IN METERS

0 · 200 · 400 · 600 · 800 · 1000 · 1200 · 1400 · 1600

Hydrothermal Gradient

Water + free gas

No gas hydrate above this depth

Phase Boundary

Water + gas hydrate

METHANE HYDRATE

Water

Gas hydrate stability zone (GHSZ)

Sediment

Geothermal Gradient

Base of Gas Hydrate

TEMPERATURE °C

-20 · -10 · 0 · 10 · 20 · 30

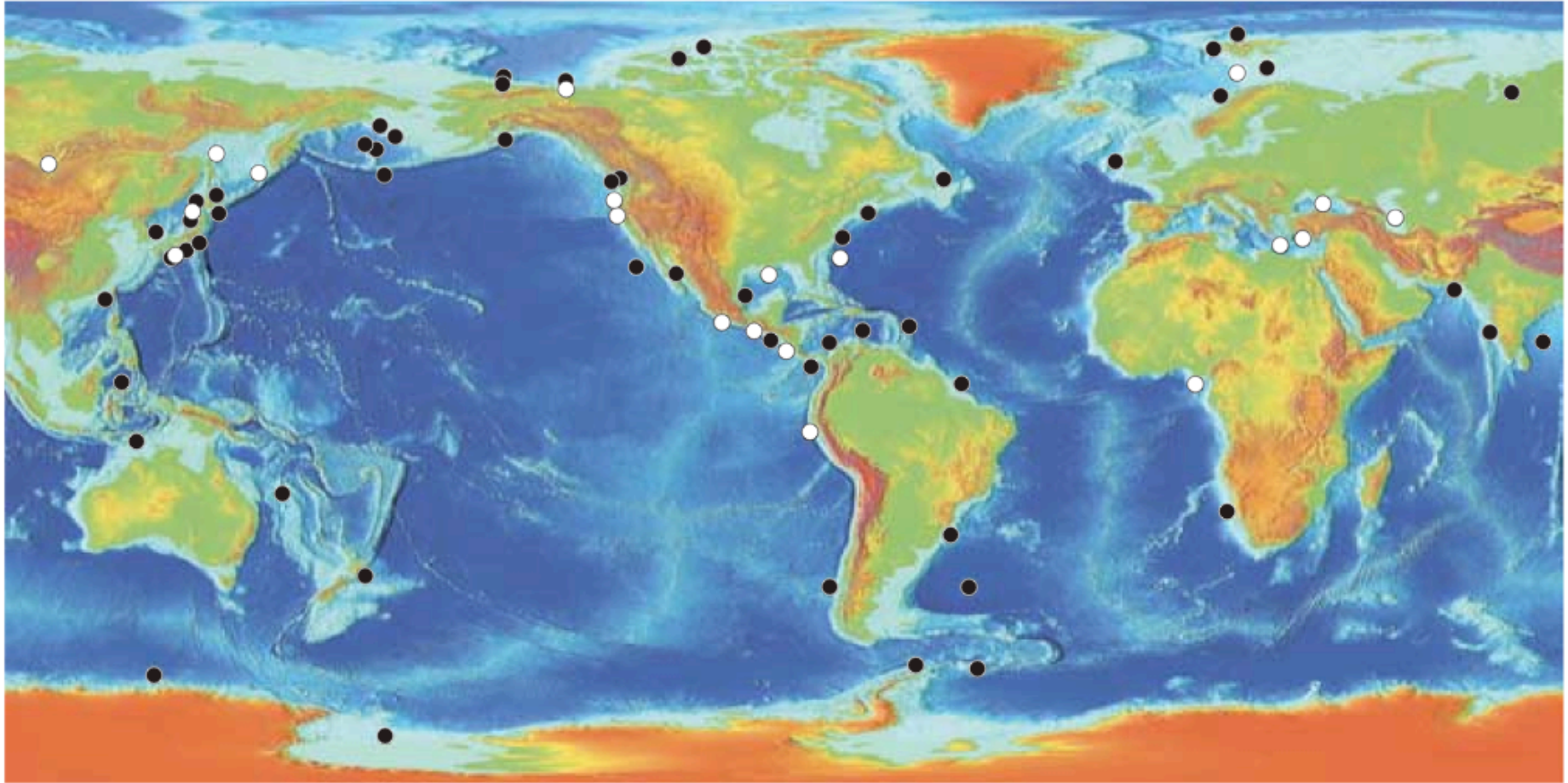Kvenvolden & Grantz, 1990

Gas hydrates are widespread

Figure 3. Gas hydrate deposits exist in about 100 separate locations throughout the world. For 20 of these sites (*white dots*), samples of hydrate have been recovered from the subsurface. For the others (*black dots*), the presence of hydrate is inferred from geophysical, geochemical or geologic evidence. (Courtesy of Keith Kvenvolden, U.S. Geological Survey.)

Kvenvolden & Lorenson, 2000

Figure 3. Photograph of a nearly pure piece of gas hydrate (Section 164-997A-42X-3; 331 mbsf) that is ~5 cm × 14 cm in size, white colored, and coated by greenish gray drilling slurry. Note the bubbles within the slurry.

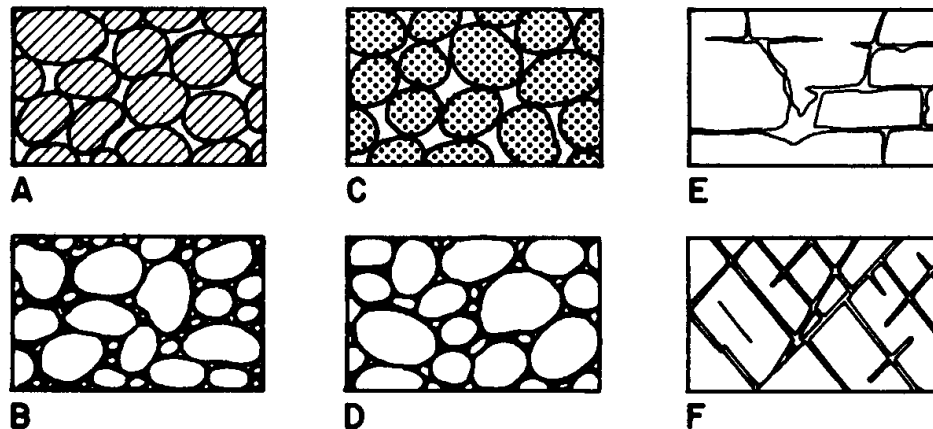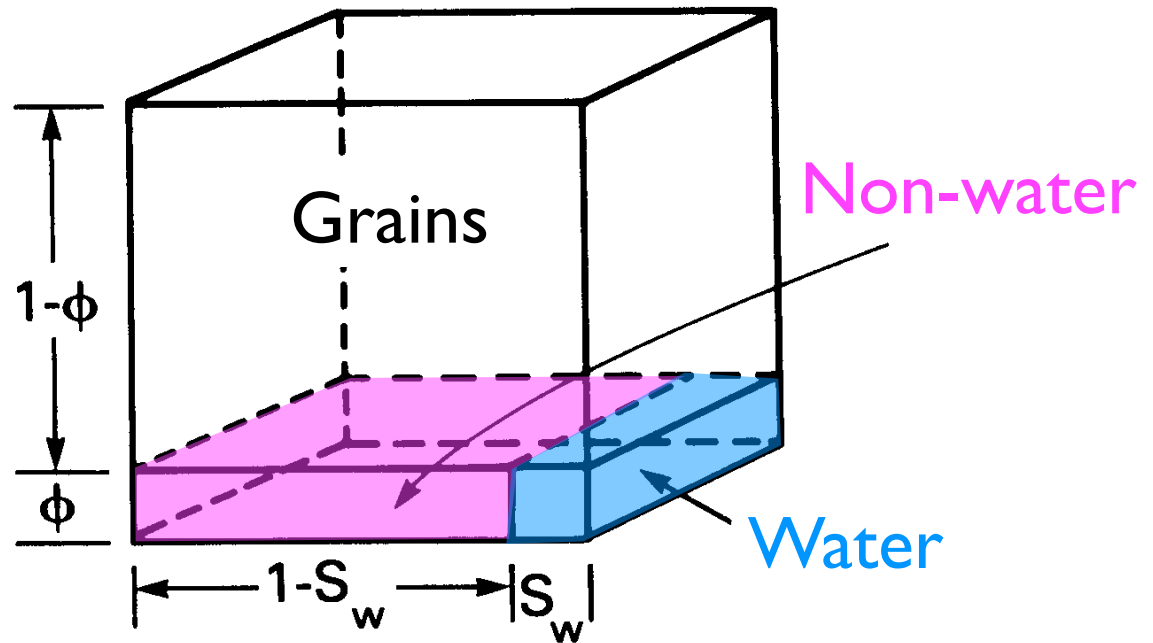$$\phi = \frac{\text{Pore volume}}{\text{Total volume}}$$

Grains

Non-water

Water

$1-\phi$

ϕ

$1-S_w$

S_w

A

C

E

B

D

F

FIG. 1.1.1. Diagram showing several types of Rock Interstices. A. Well-sorted sedimentary deposit having high porosity; B. Poorly sorted sedimentary deposit having low porosity; C. Well-sorted sedimentary deposit consisting of pebbles that are themselves porous, so that the deposit as a whole has a very high porosity; D. Well-sorted sedimentary deposit whose porosity has been diminished by the deposition of mineral matter in the interstices; E. Rock rendered porous by solution; F. Rock rendered porous by fracturing. (After Meinzer, 1942.)

TABLE III. Electrical Resistivities of Earth Materials

Material	Resistivity (Ω m at 18–20°C)	
Pure Materials[a]		
Marble	$5 \times 10^7 - 10^9$	
Mica	$10^{11} - 10^{14}$	
Quartz ∥	1×10^{12}	
Quartz ⊥	3×10^{14}	
Slate	$1 - 2 \times 10^6$	
Sulfur	$10^{14} - 10^{15}$	temperature unknown
Petroleum	2×10^{14}	temperature unknown
Distilled water	0.5×10^4	
Salt Water at 15°C[b] (kppm NaCl)		
2	3.4	
10	0.72	
20	0.38	
100	0.09	
200	0.06	
Typical Formations[c]		
Clay/shale	2–10	
Saltwater sands	0.5–10	
Oil sands	$5 - 10^3$	
Compact limestone	10^3	
Dolomite	10^3	
Lignite	10^2	

[a] "Handbook of Chemistry and Physics," 38th Ed., pp. 2237–2238. Chemical Rubber Publishing Co., Cleveland, 1956.

[b] R. Desbrandes, "Diagraphies dans les Sondages," p. 124. Éditions Technip, Paris, France, 1982.

[c] R. Desbrandes, "Théorie et Interprétation des Diagraphies," p. 8. Éditions Technip, Paris, France, 1968.

The electrical resistivity of rocks in the upper portion of the earth's crust varies with:

1. Water content. Natural waters are much more conductive than most rock-forming minerals.
2. Salinity. Natural waters are conductive in proportion to the concentration of ionized salts in the water.
3. Temperature. A rock at a depth of 1 km can be twice as conductive as the same rock at the surface because water conductivity increases with temperature.
4. Clays and conductive minerals. Clays can augment the ionic conduction of pore water. Electronic conduction in sulfide and oxide minerals can dominate if such minerals are sufficiently abundant.
5. Geologic strike of the formation. Many sedimentary and metamorphic rocks are anisotropic; they have a lower resistivity along the bedding plane than perpendicular to it.
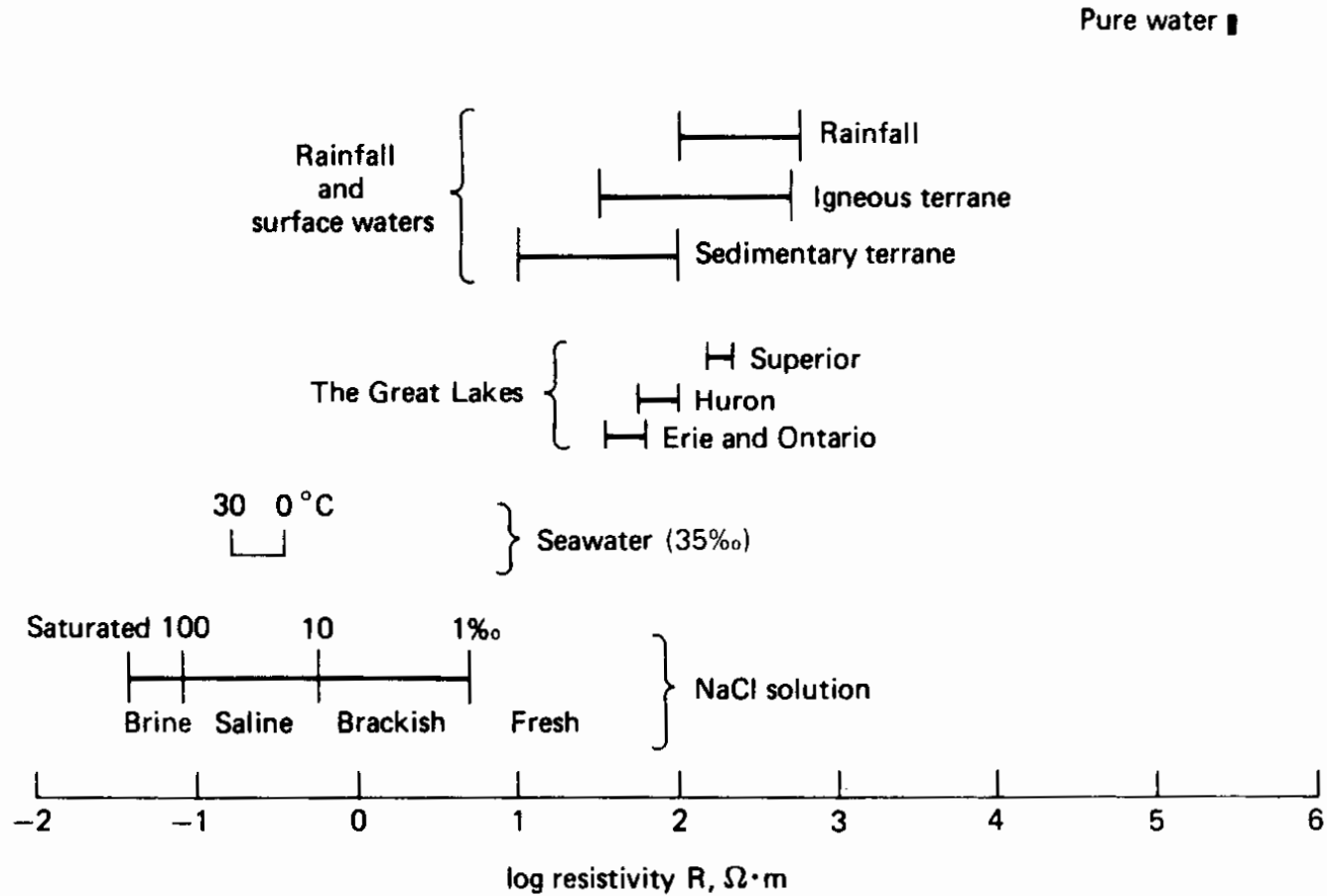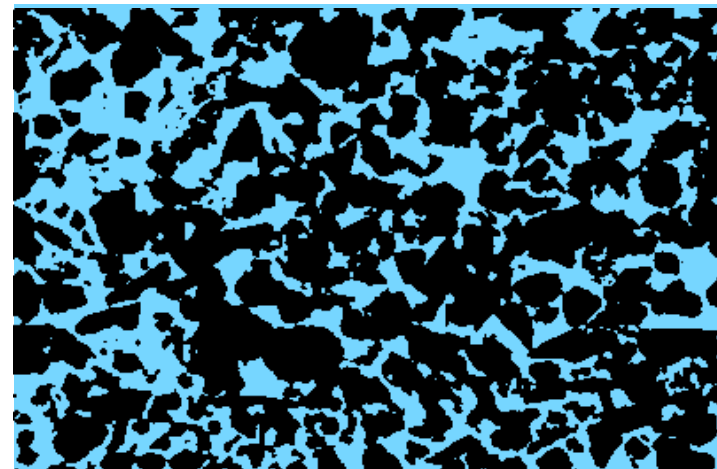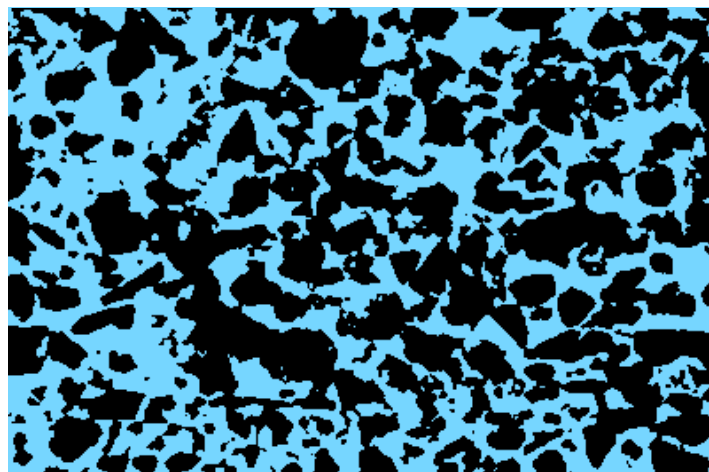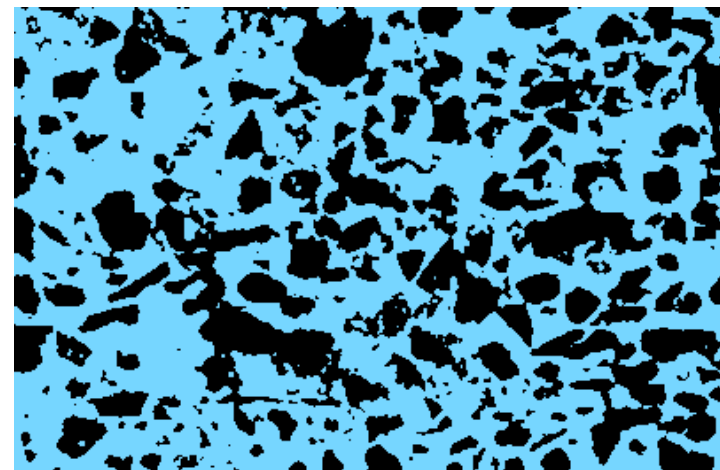
Figure 5.2   *Range of resistivity values of pure and natural waters. (Data sources: pure water, Dorsey, 1940; rainfall, Sarma and Rao, 1972; Great Lakes, Doherty, 1963; NaCl, Schlumberger, 1972; all other information, Freeze and Cherry, 1979)*
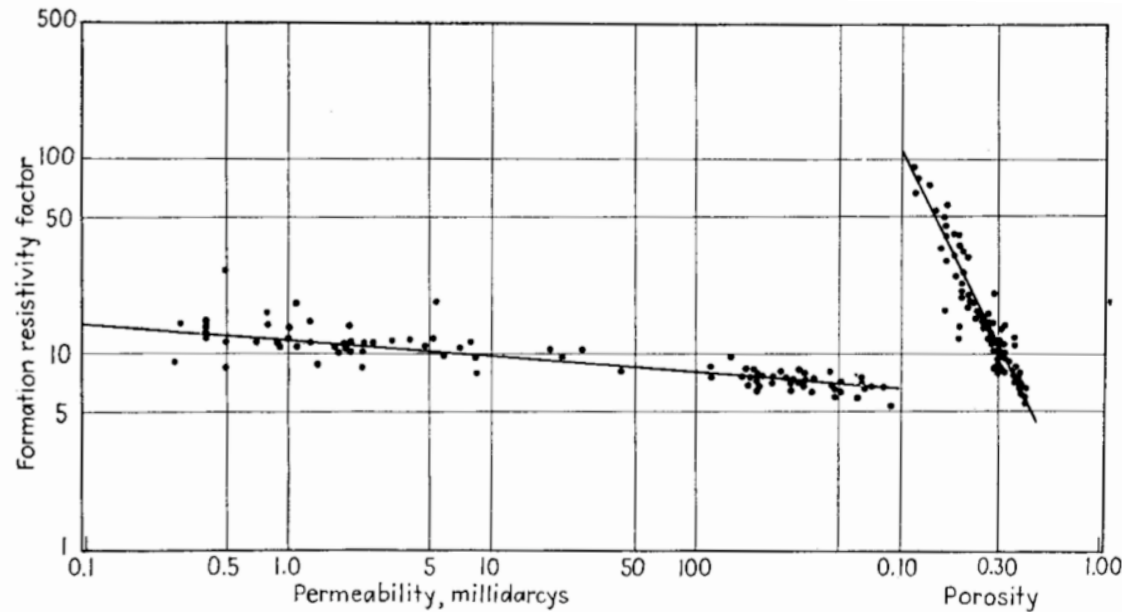
Resistivity

Water

Porosity

Archie's equation (I)

FIG. 2.—RELATION OF POROSITY AND PERMEABILITY TO FORMATION RESISTIVITY FACTOR, NACATOCH SAND, BELLEVUE, LA.

$$R_0 = FR_w = \frac{a\,R_w}{\phi^m}$$

R_0 Resistivity of fully water-saturated sample

R_w Resistivity of water

F Formation factor > 1

a Tortuosity coefficient ≈ 1

m Cementation exponent ≈ 2
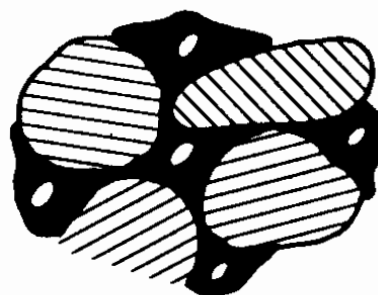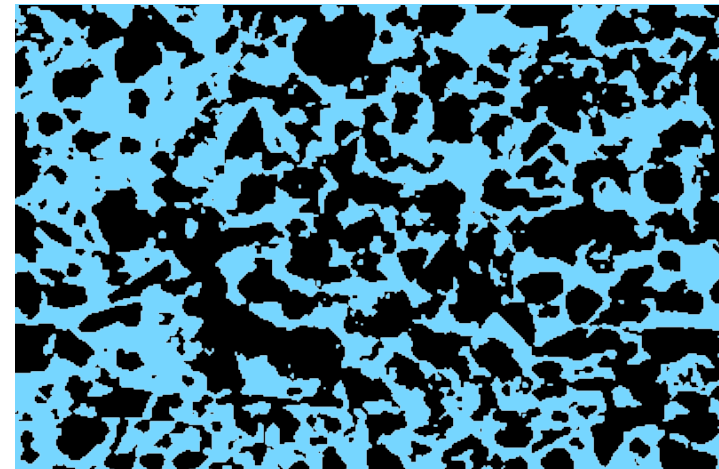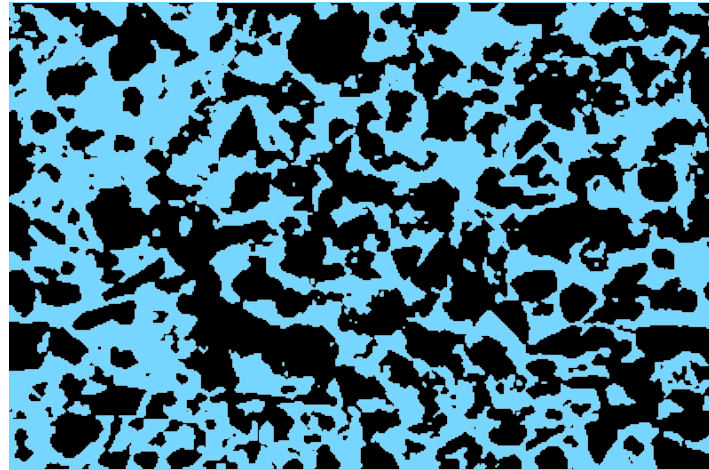
Water wet sand
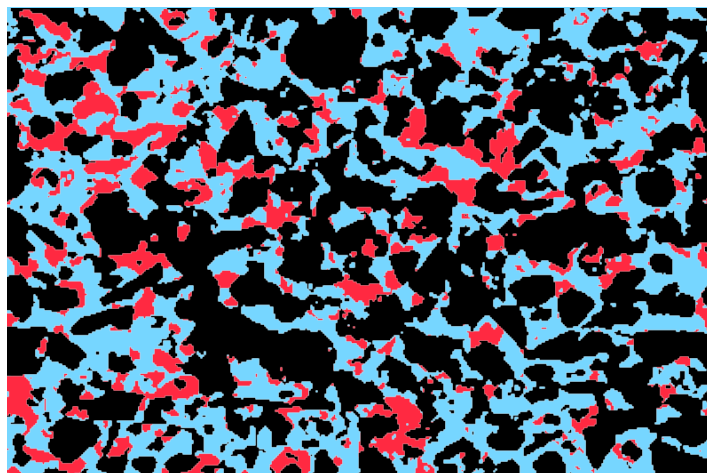
Oil wet sand
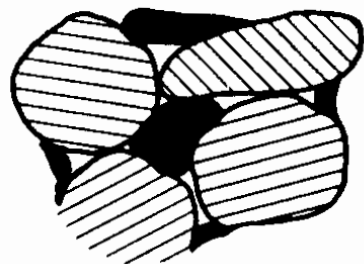
(a)
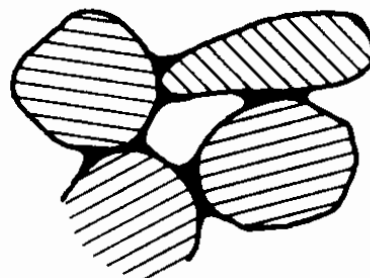
(d)
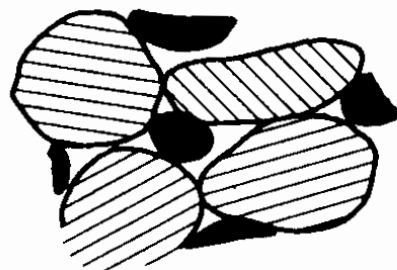
(b)
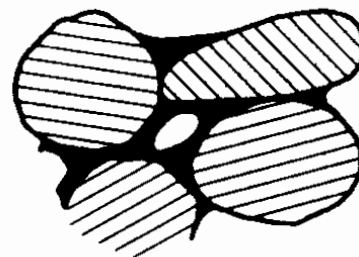
(e)
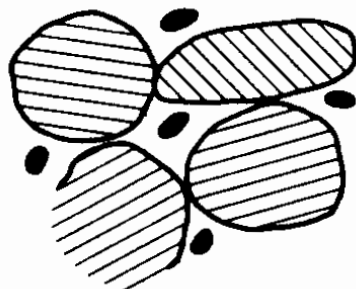
(c)

(f)

Water

Oil

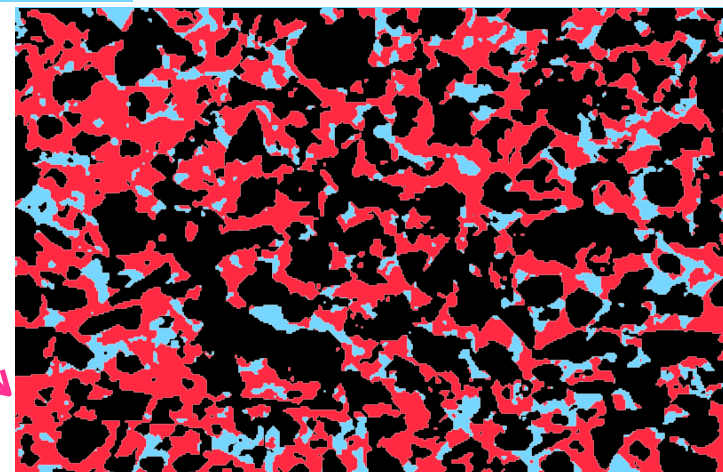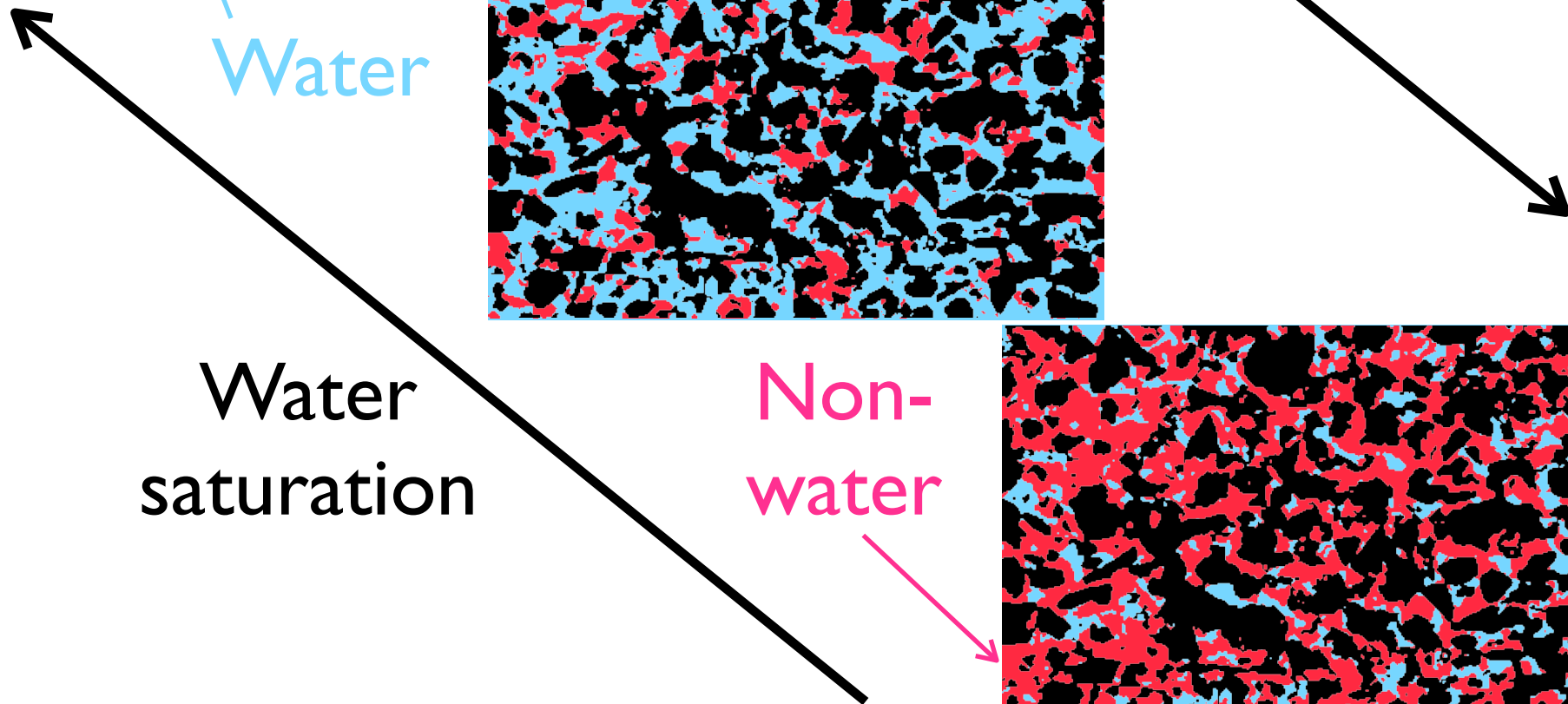Constant
resistivity

Constant
porosity

Resistivity

Water

Water
saturation

Non-
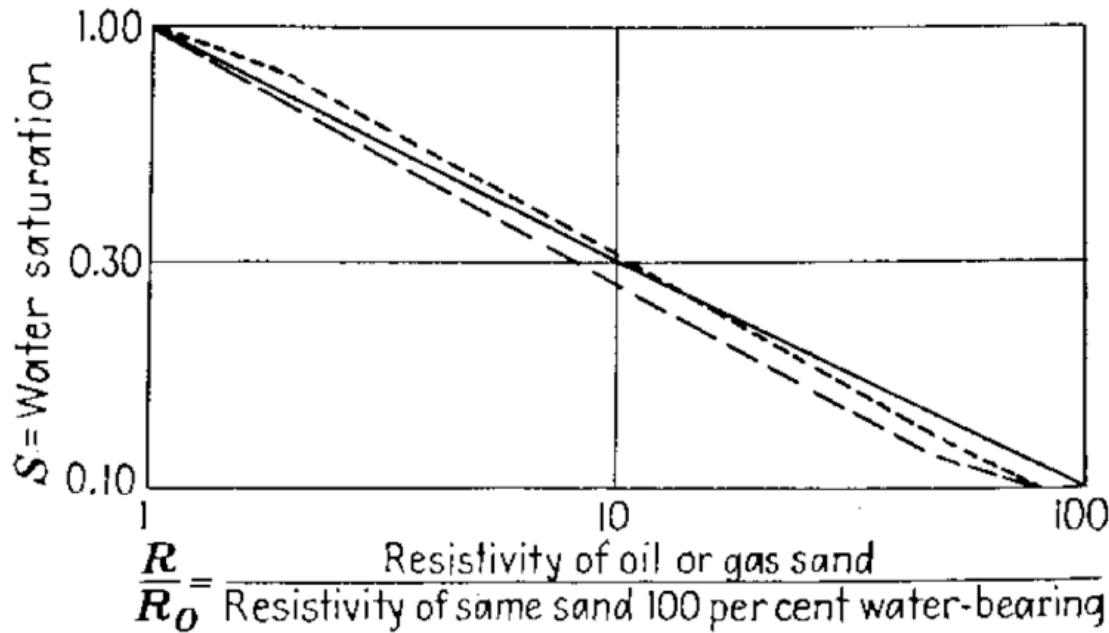water
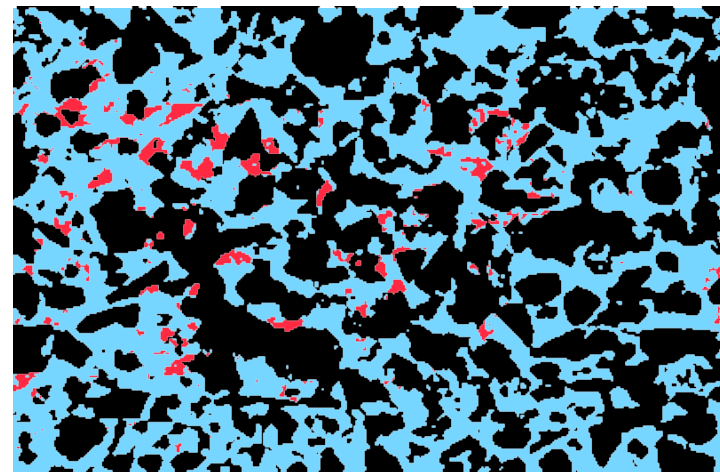
Archie's equation (2)

$$R_t = \frac{R_0}{(S_w)^n}$$

R_0 Resistivity of fully water-saturated sample

R_w Resistivity of water

R_t Resistivity of sample

S_w Water saturation of sample

F Formation factor > 1

a Tortuosity coefficient ≈ 1

m Cementation exponent ≈ 2

n Saturation exponent ≈ 2

Archie's equation

$$S_w = \left[\frac{a\,R_w}{\phi^m R_t} \right]^{1/n}$$

$$R_0 = \frac{a\,R_w}{\phi^m} \qquad R_t = \frac{R_0}{(S_w)^n}$$

R_0 Resistivity of fully water-
    saturated sample

R_w Resistivity of water
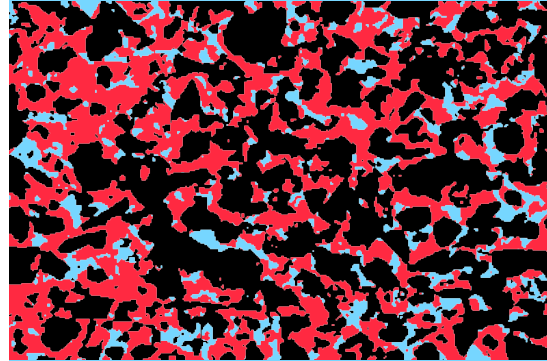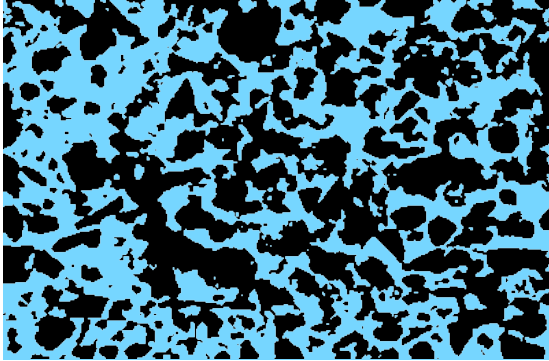
R_t Resistivity of sample

S_w Water saturation of sample

F Formation factor > 1

a Tortuosity coefficient ≈ 1
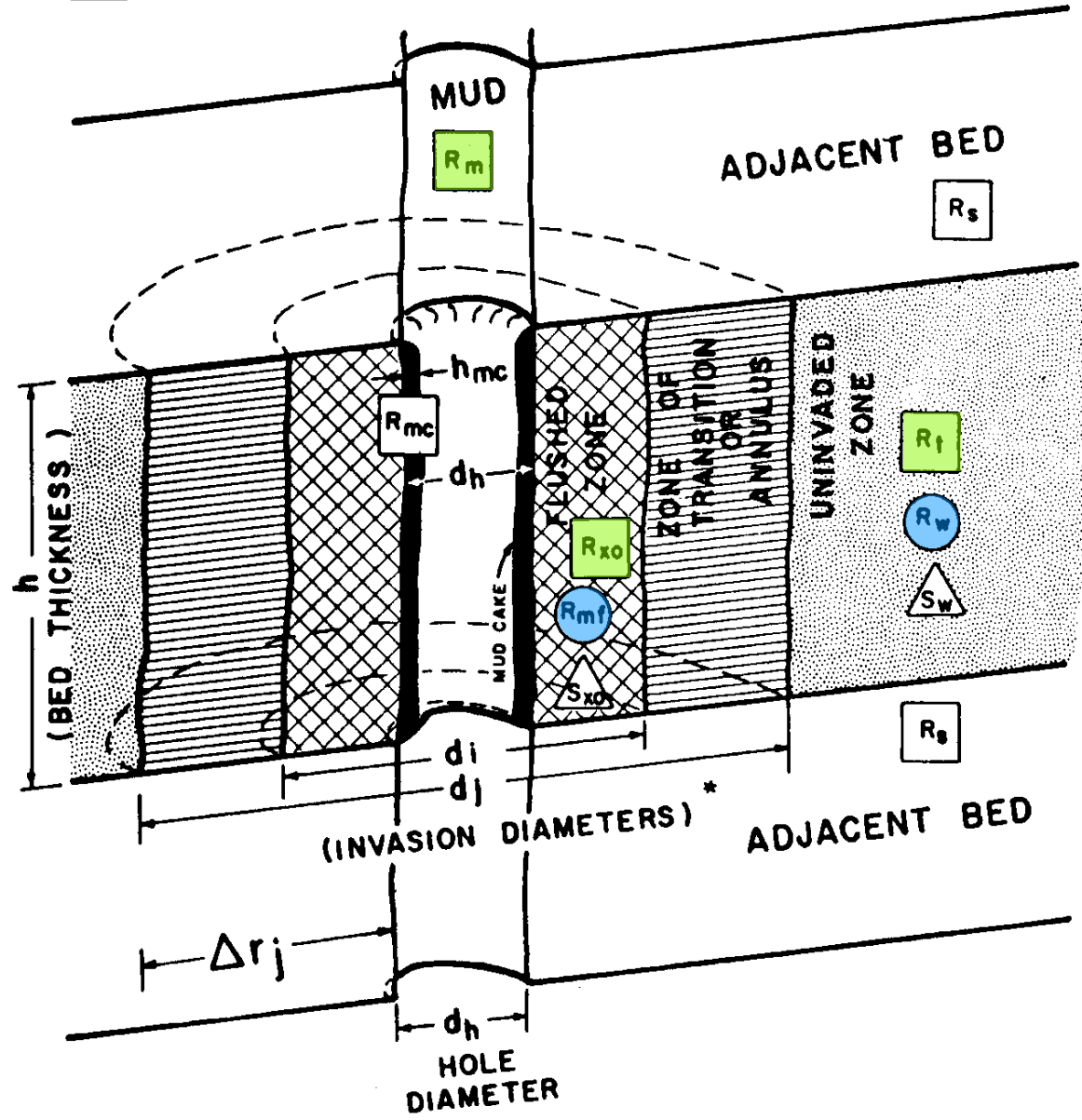
m Cementation exponent ≈ 2

n Saturation exponent ≈ 2
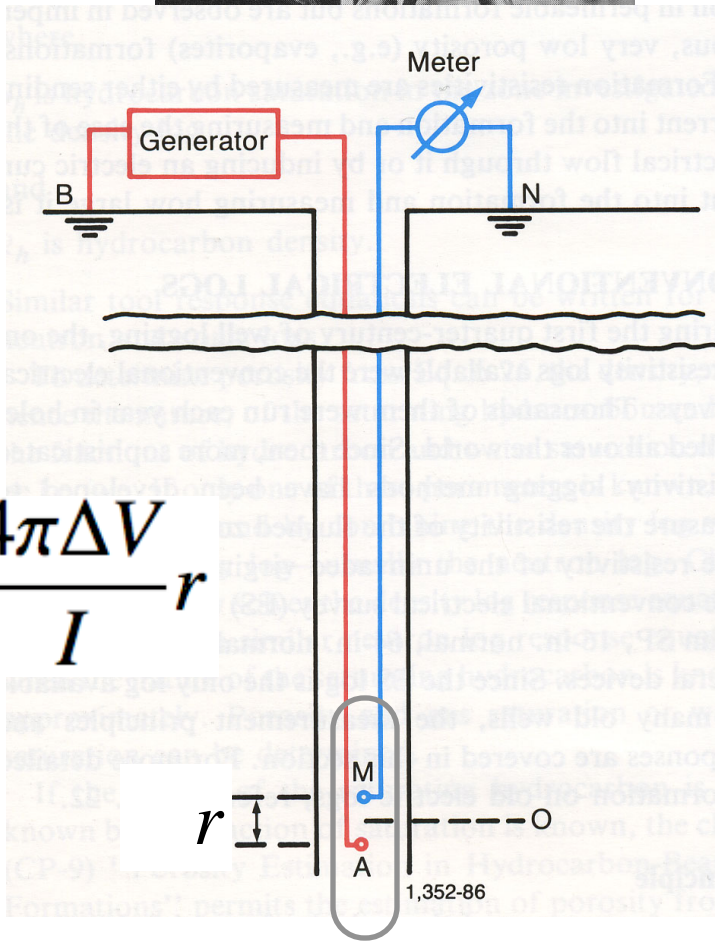
Needed for evaluation

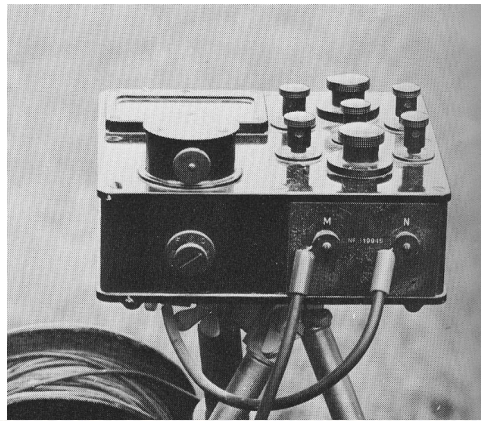$$S_w = \left[\frac{a\, R_w}{\phi^m R_t} \right]^{1/n}$$

- Porosity and "true" formation resistivity (from downhole logs)
- Formation water resistivity (from local pore water salinity and temperature)
- Coefficients a, m, and n
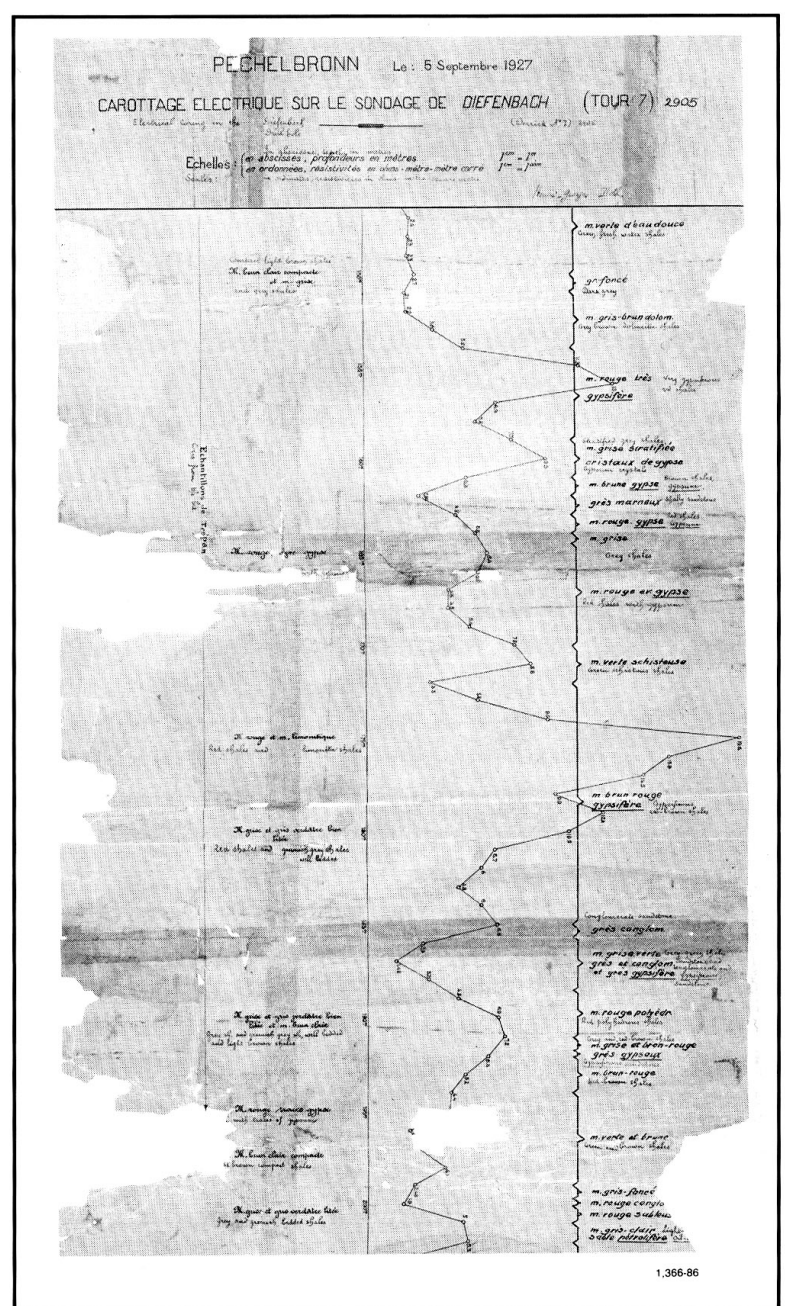
1927

$$R_a = \frac{4\pi\Delta V}{I} r$$

Fig. 1-1—The first log: points plotted on graph paper by Henri Doll.
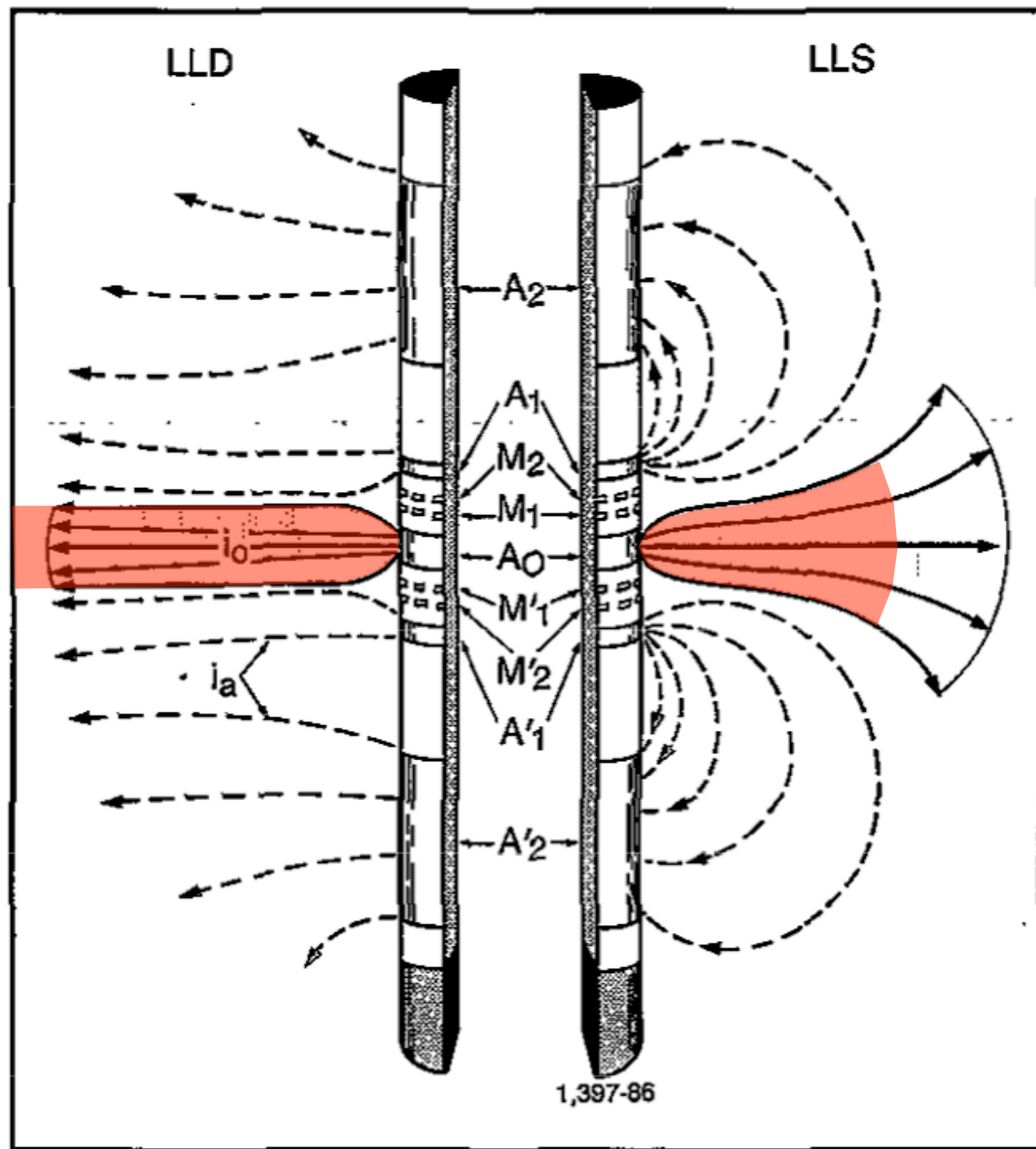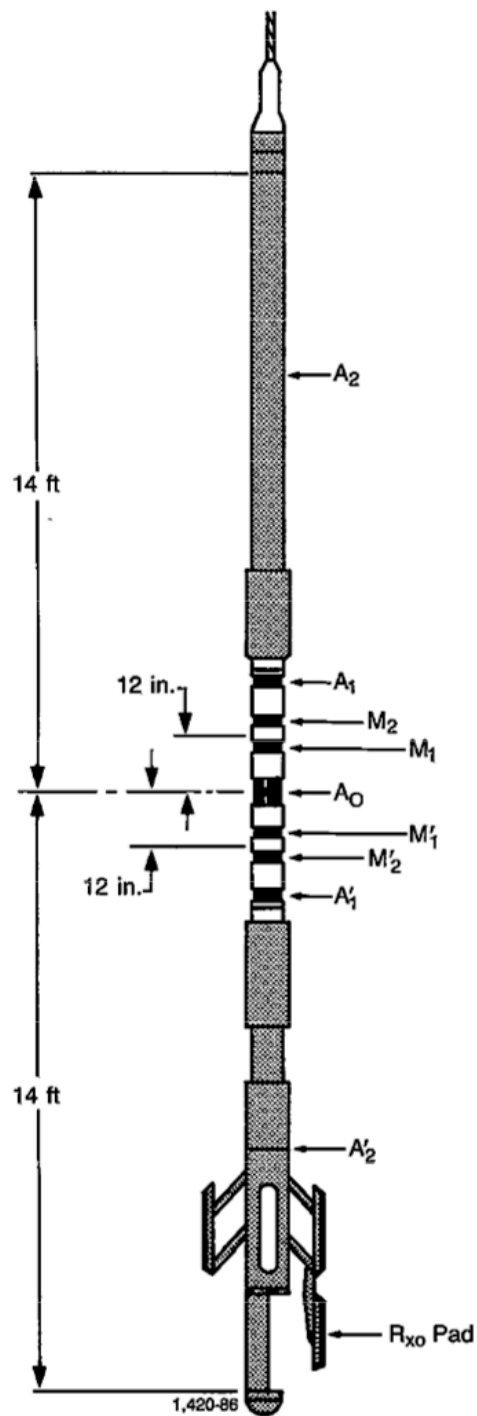
Fig. 7-13—Schematic of the Dual Laterolog.

Upper transmitter

Azimuthal electrodes

Ring electrode

Lower transmitter

56 samples

RAB Image

Top   Bottom   Top

FMI Image

Top   Bottom   Top

Depth 10 ft
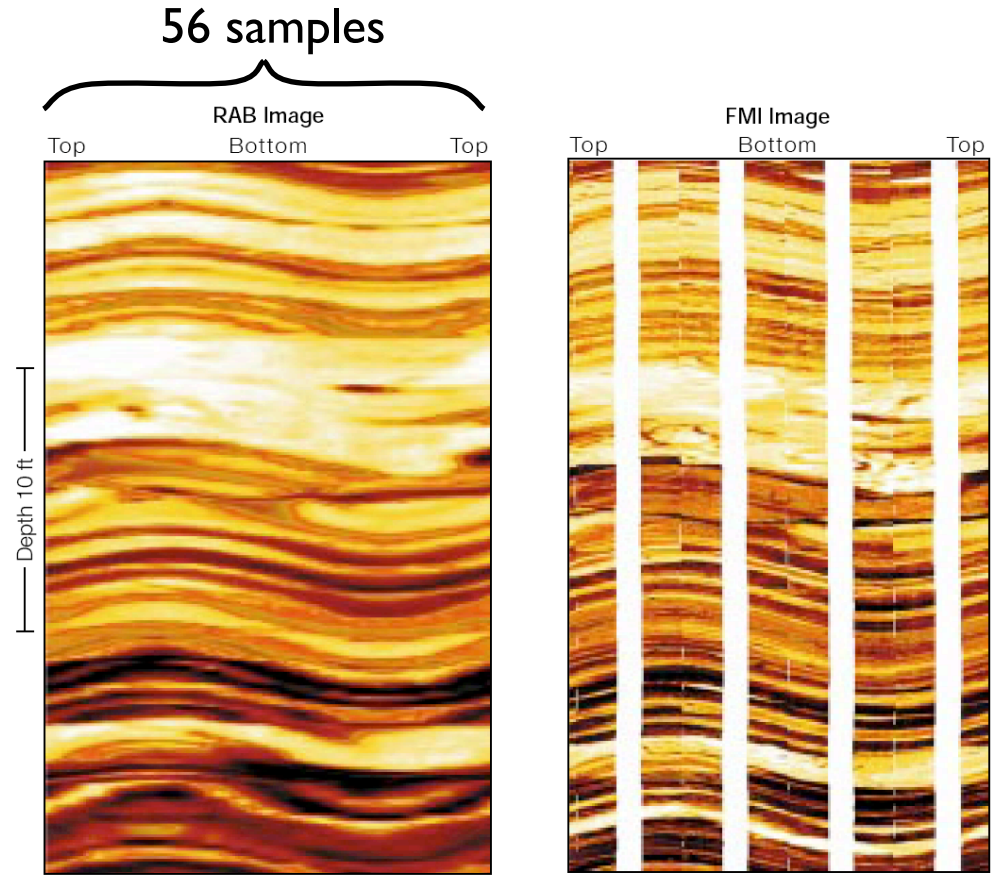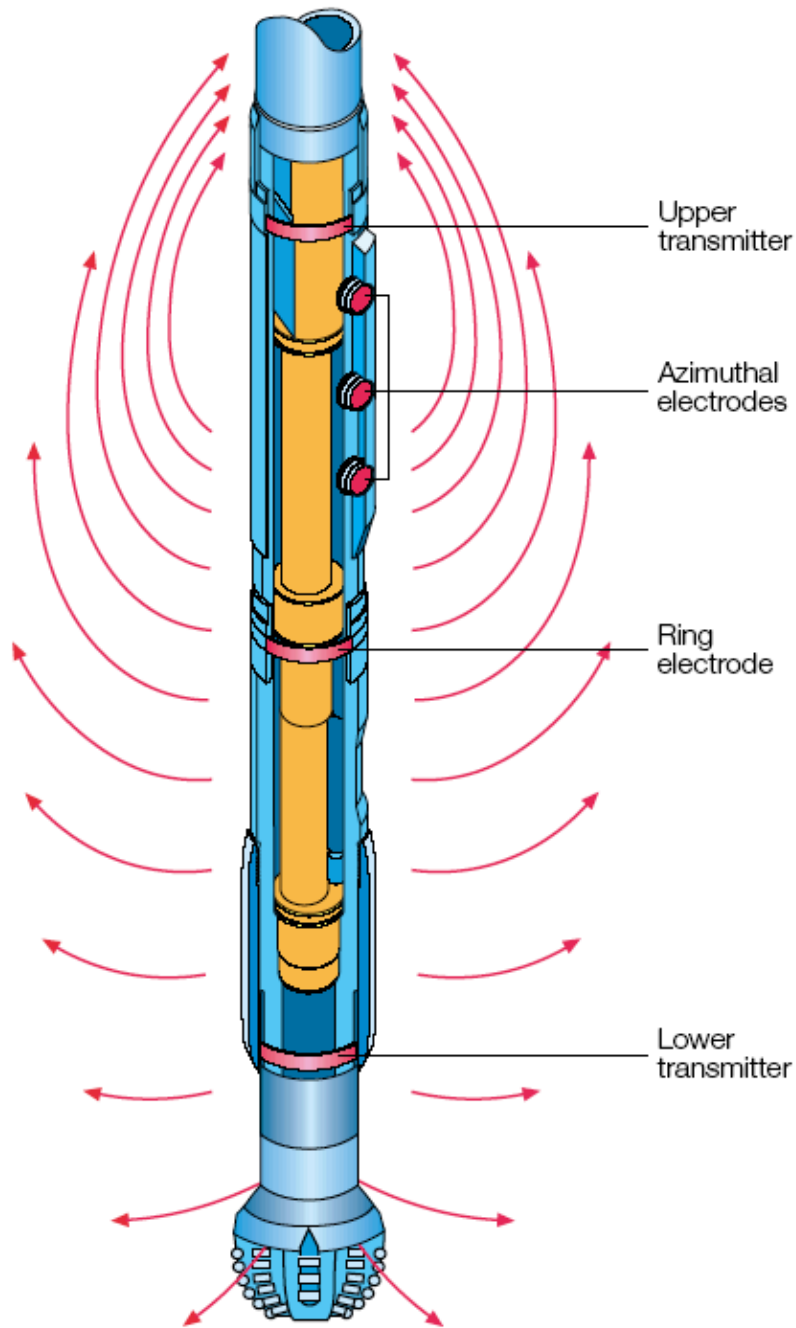
RAB and FMI images of dipping beds. Both RAB and FMI images show large-scale events that are several feet long. However, the resolution of the FMI image is much better. Beds less than about 4 in. [10 cm] thick are not clearly seen on the RAB image.

Porosity

Resistivity (ohm m)

GH saturation

a

b

c

R_0

R_t

GH

Depth (mbsf)
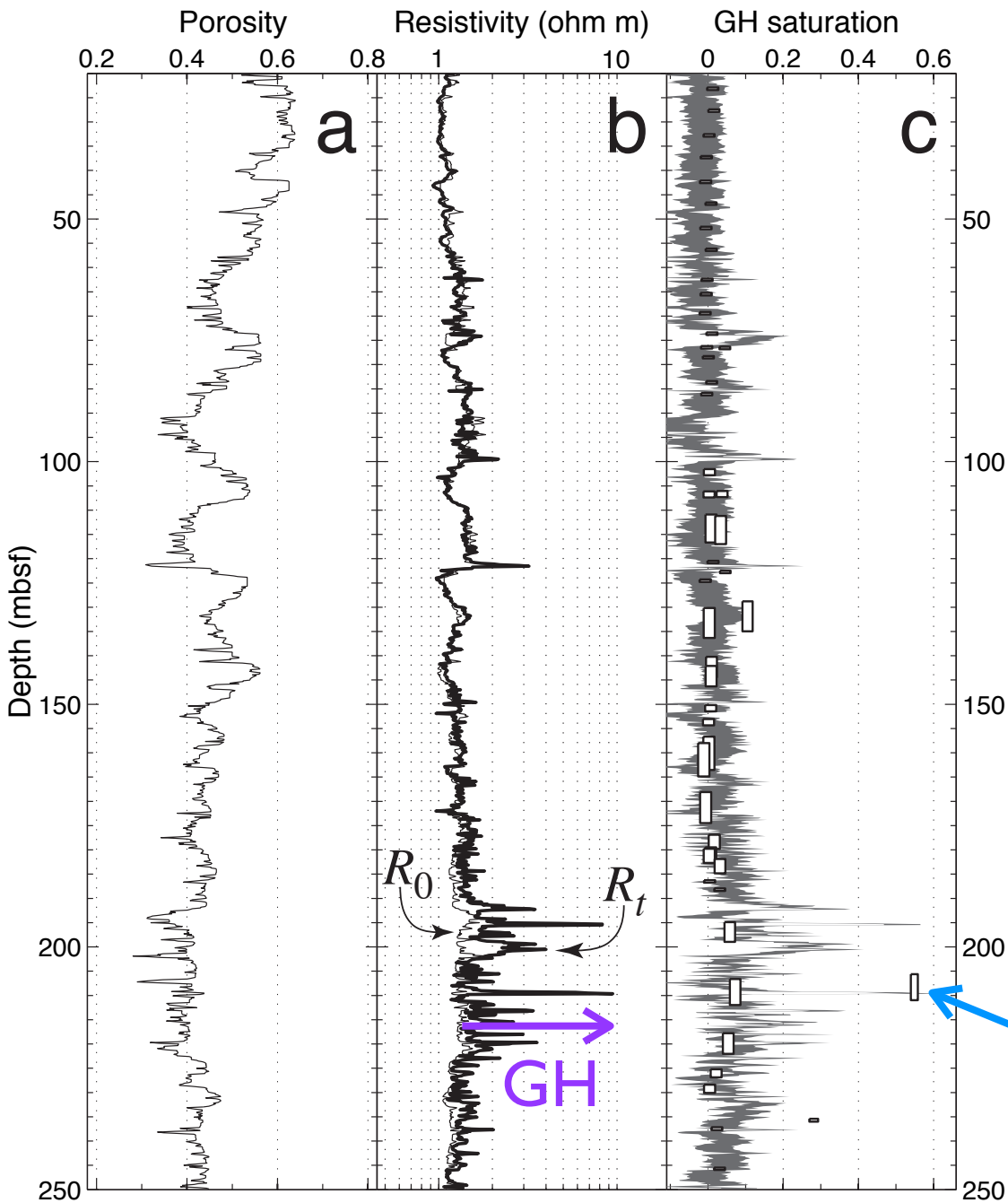
$$S_h = 1 - \left[\frac{a\, R_w}{\phi^m R_t} \right]^{\frac{1}{n}}$$

R_w from measured T and salinity baseline

$a = 2.14$, $m = 1.07$ from fitting R_0 to R_t (20-190 mbsf)

$n = 2.42 \pm 0.28$ from matching chlorinity results in 9 cm-thick sand

$$V_P = \sqrt{\frac{K + \frac{4}{3}\mu}{\rho}} \qquad V_S = \sqrt{\frac{\mu}{\rho}}$$

Compressional (P) waves
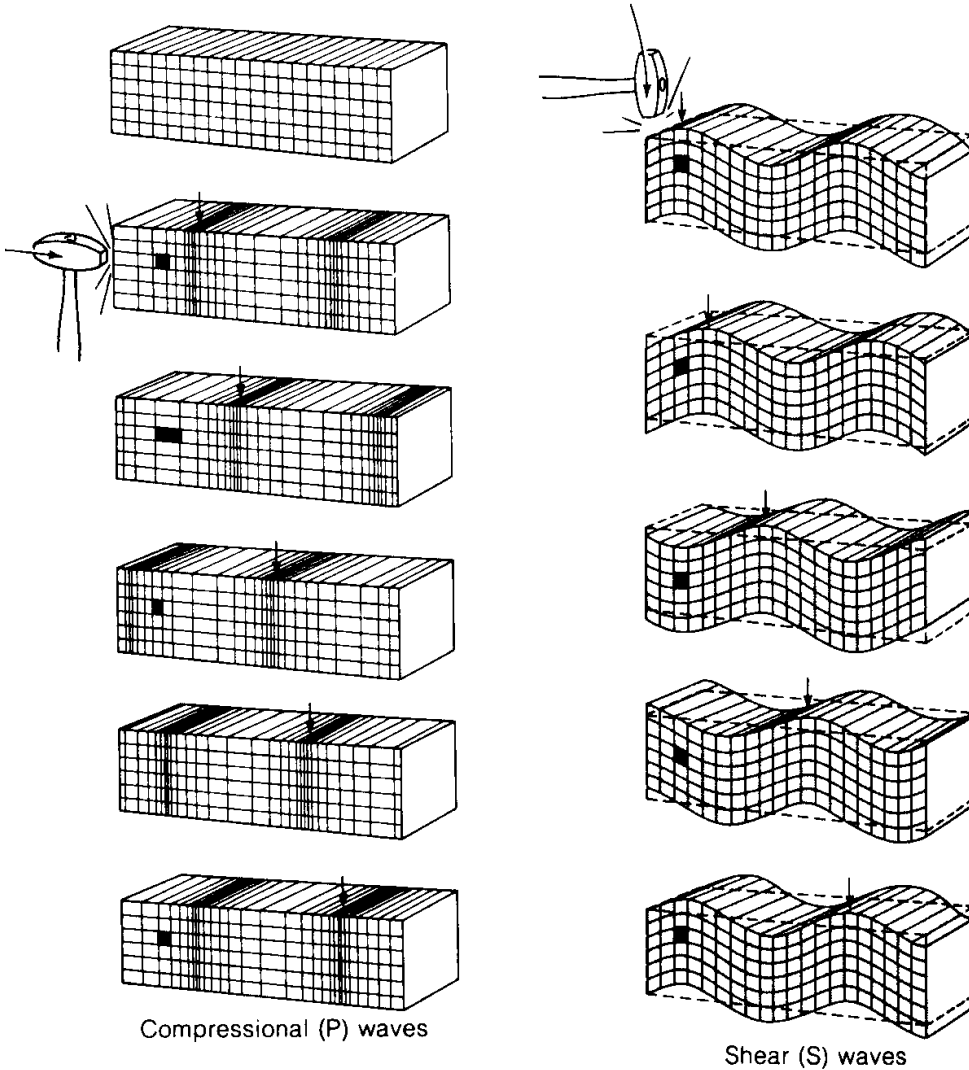
Shear (S) waves

Bulk modulus K relates compressional stress and strain

Shear modulus μ relates shear stress and strain

Table VII.4. BASIC RELATIONS BETWEEN ACOUSTIC, ELASTIC, AND MICROSTRUCTURAL PARAMETERS OF A POROUS MEDIUM

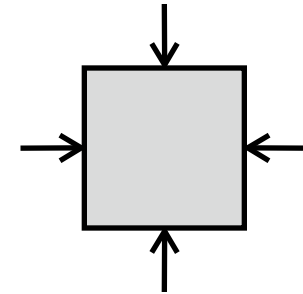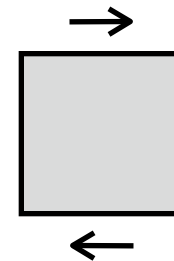|	*Porous Medium without Fluid*	*Porous Medium with Fluid*
Bulk Modulus	$K = K_s\left(1 - \beta\dfrac{\phi}{A}\right)$	$K_u = K + \dfrac{K_f\left(1 - \dfrac{K}{K_s}\right)^2}{\phi + \left(1 - \dfrac{K}{K_s} - \phi\right)\dfrac{K_f}{K_s}}$
Shear Modulus	$\mu = \mu_s\left(1 - \beta'\dfrac{\phi}{A}\right)$	$\mu_u = \mu$
Density	$\rho = \rho_s(1 - \phi)$	$\rho' = \rho_s(1 - \phi) + \rho_f\phi$
P = Wave	$V_p = \left(\dfrac{K + (4/3)\mu}{\rho}\right)^{1/2}$	$V_p = \left(\dfrac{K_u + (4/3)\mu}{\rho'}\right)^{1/2}$
S-Wave	$V_s = \left(\dfrac{\mu}{\rho}\right)^{1/2}$	$V_s = \left(\dfrac{\mu}{\rho'}\right)^{1/2}$

K_s, μ_s Elastic moduli of the rock grains

K_f Bulk modulus of fluid

ρ_s, ρ_f Rock grain and fluid densities

A Pore shape aspect ratio ≤ 1

β, β' ≈ 1

Contact Cementing

Grain Coating

Matrix Supporting

**Pore Filling**
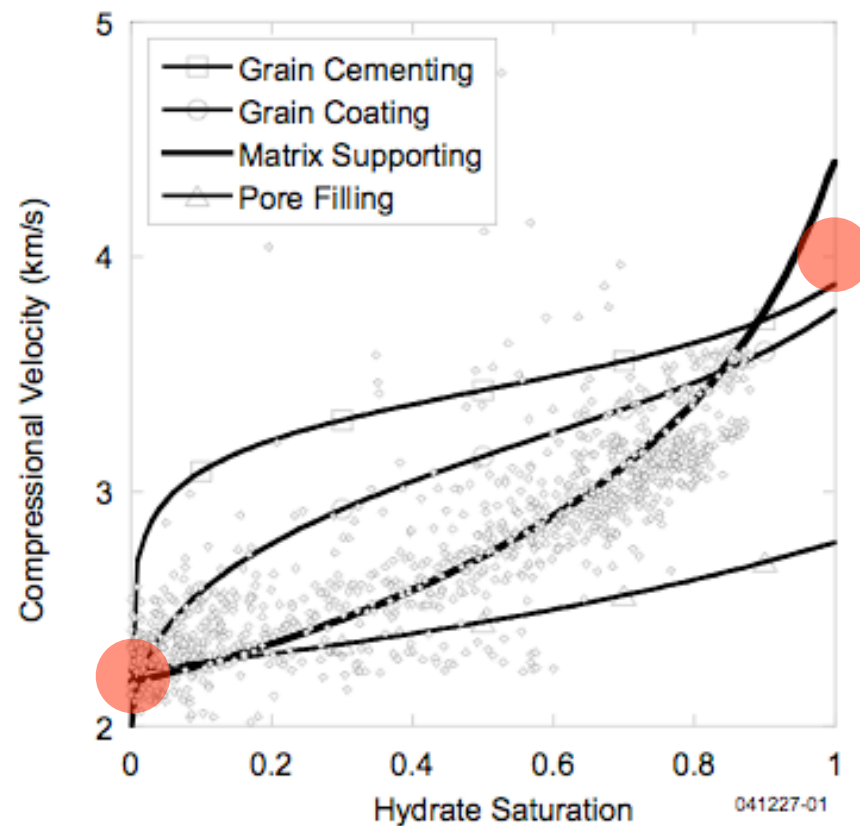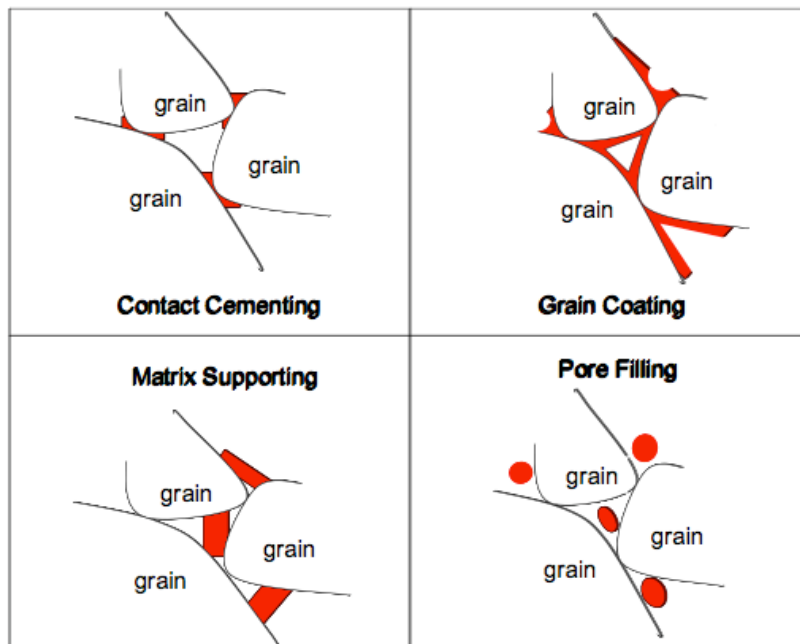
Kleinberg &
Dai, 2005

Figure 11a. Well log measurements of compressional wave speed [Reference 2] compared to the predictions of four growth habit models.
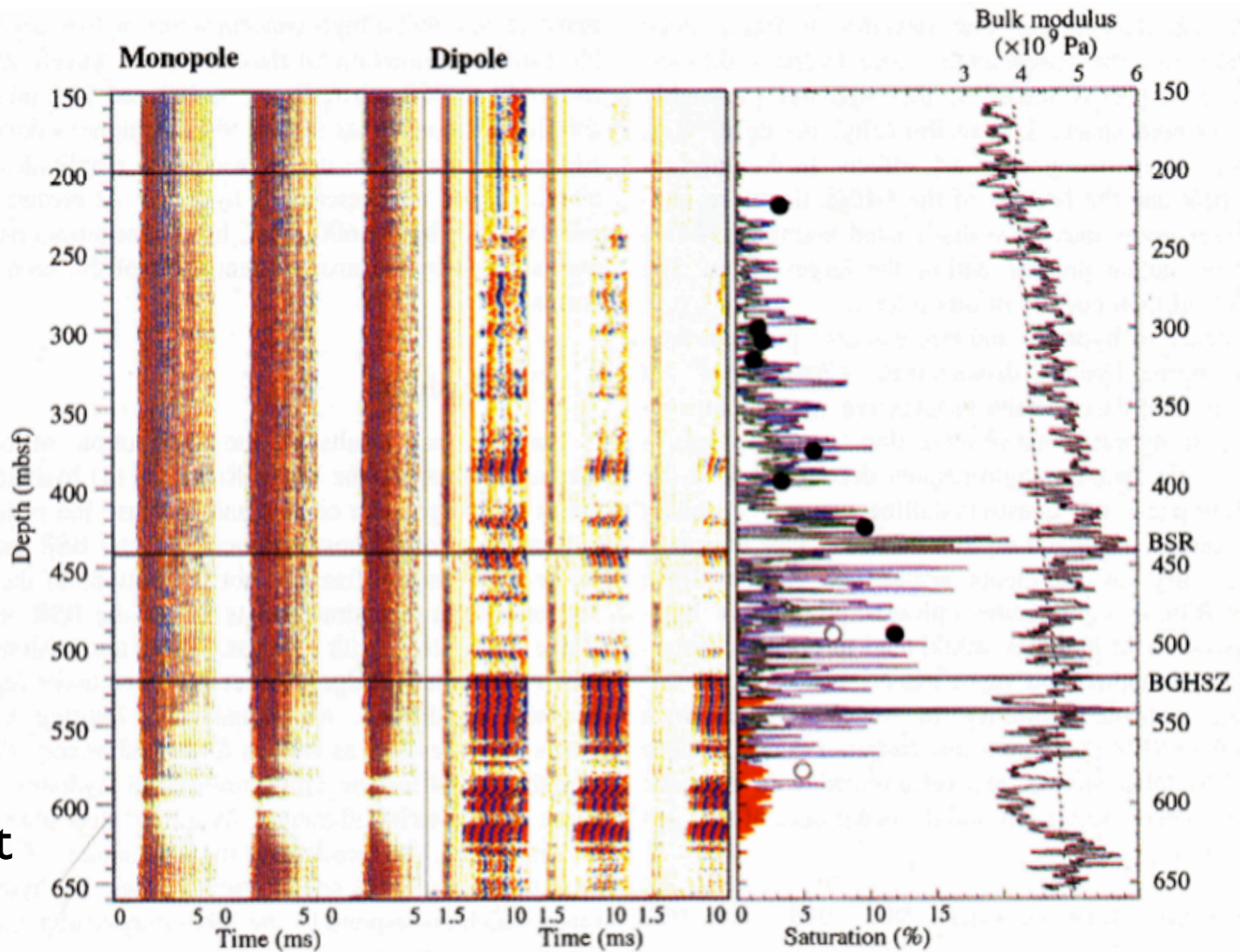
Guerin et al. 1999

Plate 2. Summary of results from Plate 1 and Figures 5 and 7, linking the sonic logging waveforms and the bulk modulus to the methane saturation estimates of free gas and gas hydrate (see text). Methane saturation from cementation theory for hydrates uniformly deposited on the grains (blue line), free gas concentration below the GHSZ (red fill), and hydrate concentration between the BSR and the BGHSZ assuming that 1% of the pore space is occupied by free gas (purple line). The green line gives the result of the cementation theory calculated from density and porosity data measured on cores. Circles are PCS results. Bulk modulus K (solid black line) and the Gassmann/Hamilton model (dotted line) are also shown. Gas hydrate is present where K is significantly higher than this model, while free gas is indicated by lower values of K.
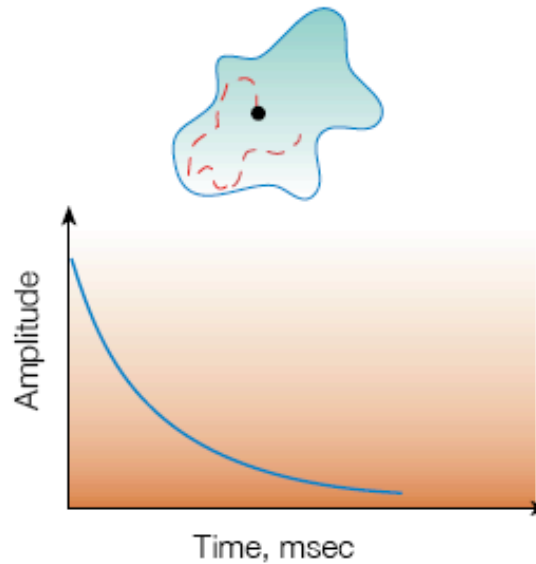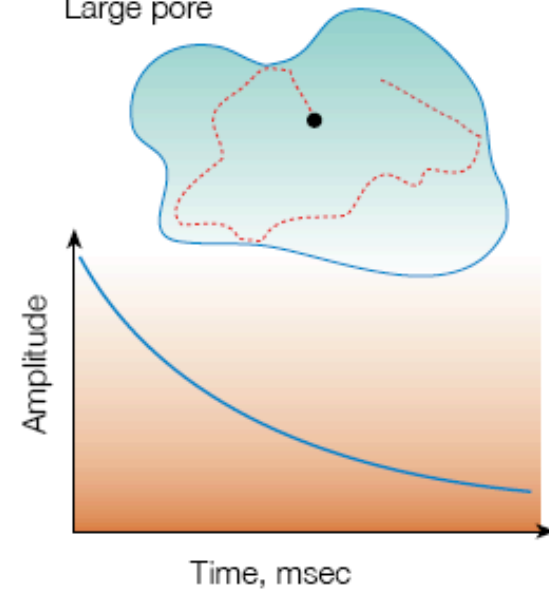
Nuclear magnetic resonance
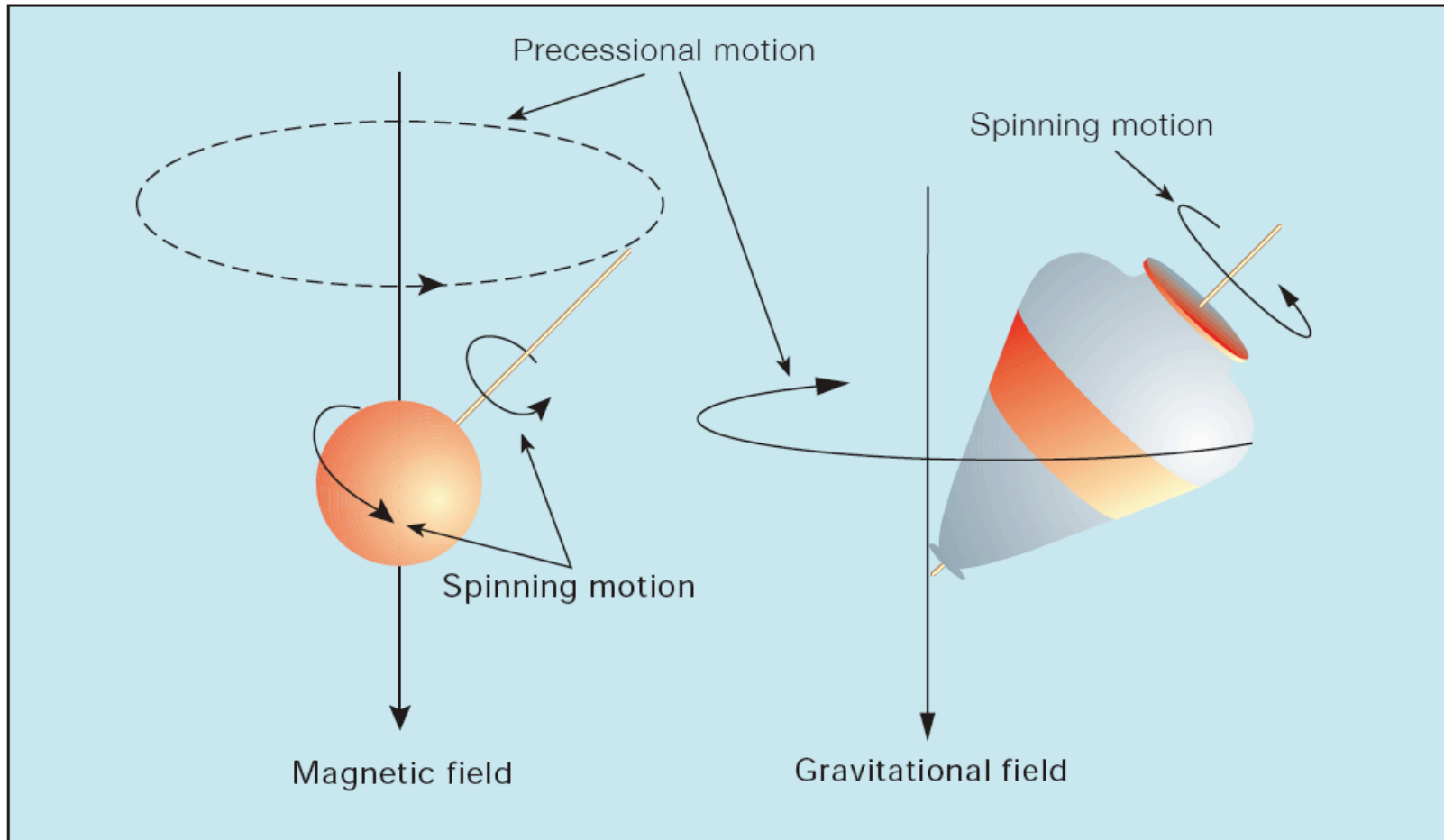
Precessing protons. Hydrogen nuclei—protons—behave like spinning bar magnets. Once disturbed from equilibrium, they precess about the static magnetic field (left) in the same way that a child's spinning top precesses in the Earth's gravitational field (right).
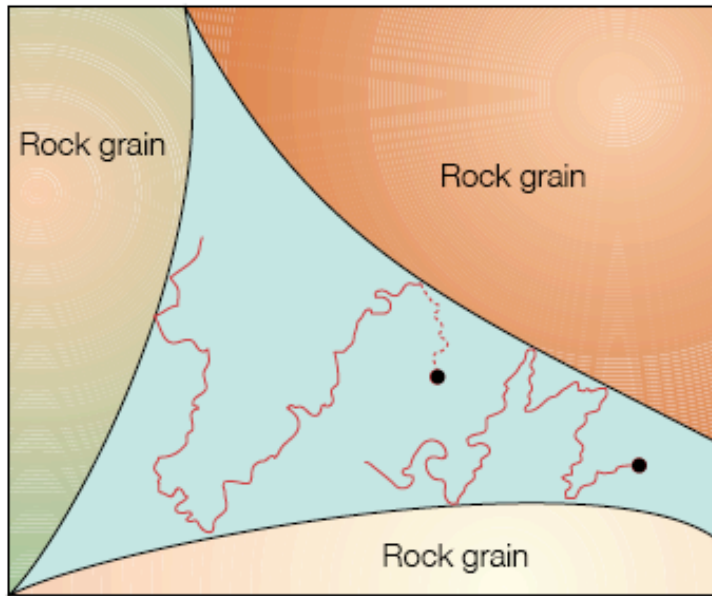
Grain surface relaxation. Precessing protons move about pore space colliding with other protons and with grain surfaces *(left)*. Every time a proton collides with a grain surface there is a possibility of a relaxation interaction occurring. Grain surface relaxation is the most important process affecting T_1 and T_2 relaxation times. Experimenters have shown that when the probability of colliding with a grain surface is high—small pores *(center)*—relaxation is rapid and when the probability of colliding with a grain surface is low—large pores *(right)*—relaxation is slower.

Φ_{NMR}

$T_2 = 5$ ms $T_2 = 20$ ms $T_2 = 80$ ms
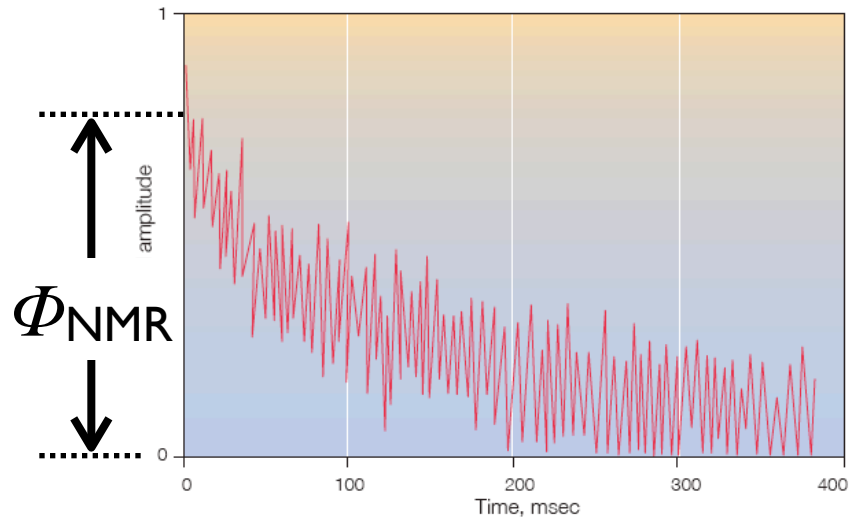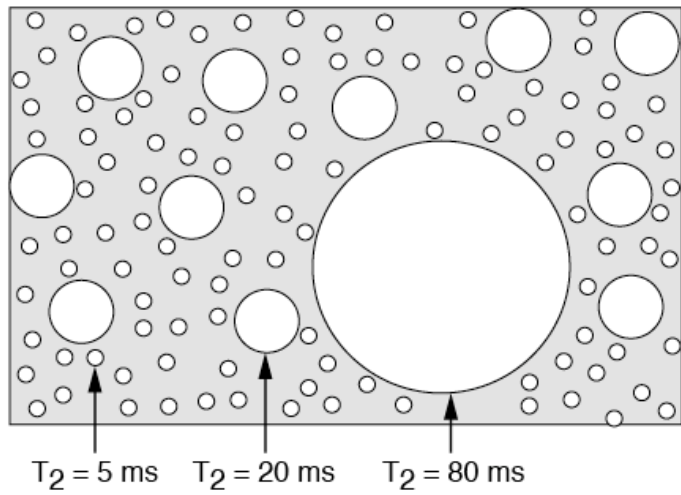
Signal amplitude processed to give T_2 distribution. The CMR tool measures decaying NMR signal amplitude (top), which is the sum of all the decaying T_2 signals generated by hydrogen protons in the measurement volume. Separating out ranges of T_2 values by a mathematical inversion process produces the T_2 distribution (bottom). The curve represents the distribution of pore sizes, and the area under the curve is CMR porosity. Interpretation of pore size distribution and logarithmic mean T_2 are used to calculate such parameters as permeability and free-fluid porosity.
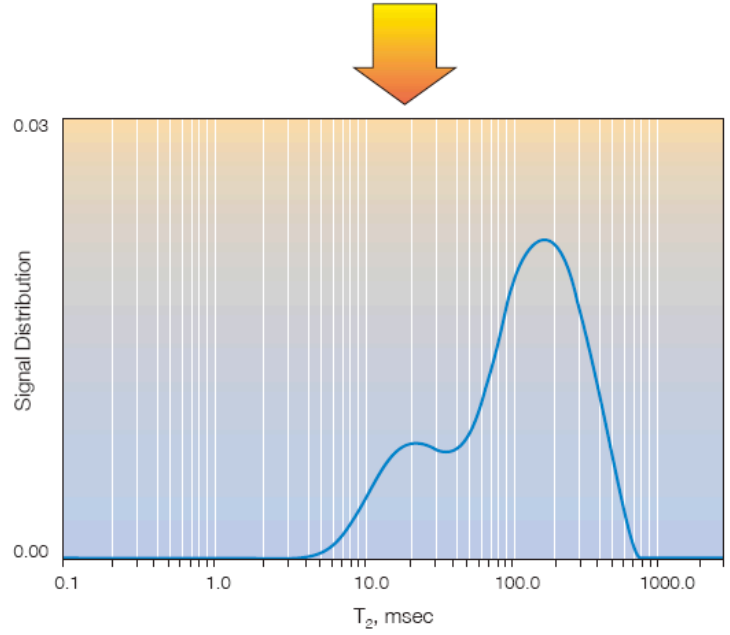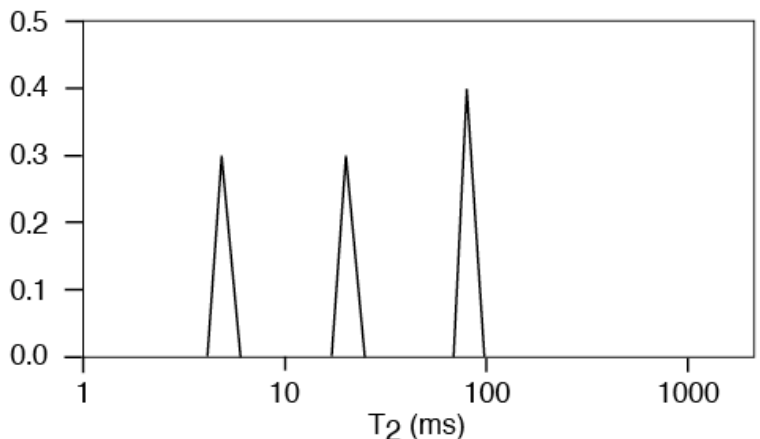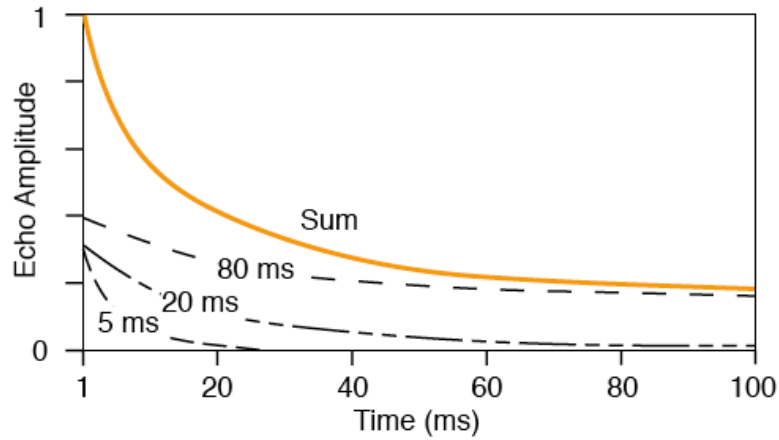
NMR porosity = fluid porosity

Legend:
- **Density Porosity** (red)
- **Neutron Porosity (Clay Corrected)** (blue dashed)
- **Magnetic Resonance Porosity** (black)
- **Sonic Slowness** (green)

50 ... (pu) ... 0

Hydrate
$$\phi_D = \phi$$
$$\phi_N = \phi \cdot 1.05$$
$$\phi_{TCMR} = 0$$

Gas
$$\phi_D = \phi + \text{gas effect}$$
$$\phi_N = \phi \cdot HI_g$$
$$\phi_{TCMR} = \phi \cdot HI_g \cdot P_g$$
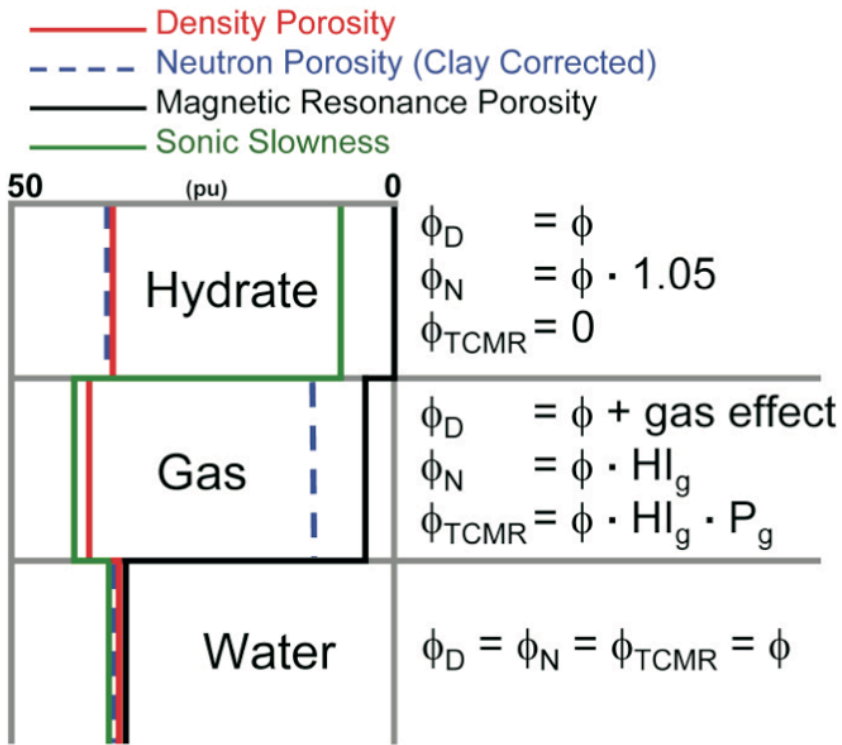
Water
$$\phi_D = \phi_N = \phi_{TCMR} = \phi$$

FIG. 1   Hypothetical porosity log responses passing through a clean reservoir with porosity of 40 p.u. The reservoir is fully saturated with hydrate (top), with gas (middle) and with water (bottom) in this idealized example.

FIG. 3   Log responses in a hydrate zone. Yellow shading in Track 3 represents the difference between ϕ_{DMR} and ϕ_{TCMR}, which is approximately the volume of gas hydrate. Track 4 shows the water saturations computed using the DMR and resistivity techniques. Spikes in DMR porosity, track 3, and in the differences between DMR and resistivity estimates of water saturation, track 4, are strongly correlated with borehole washouts, shown as blue shading in track 1.

Murray et al., 2000
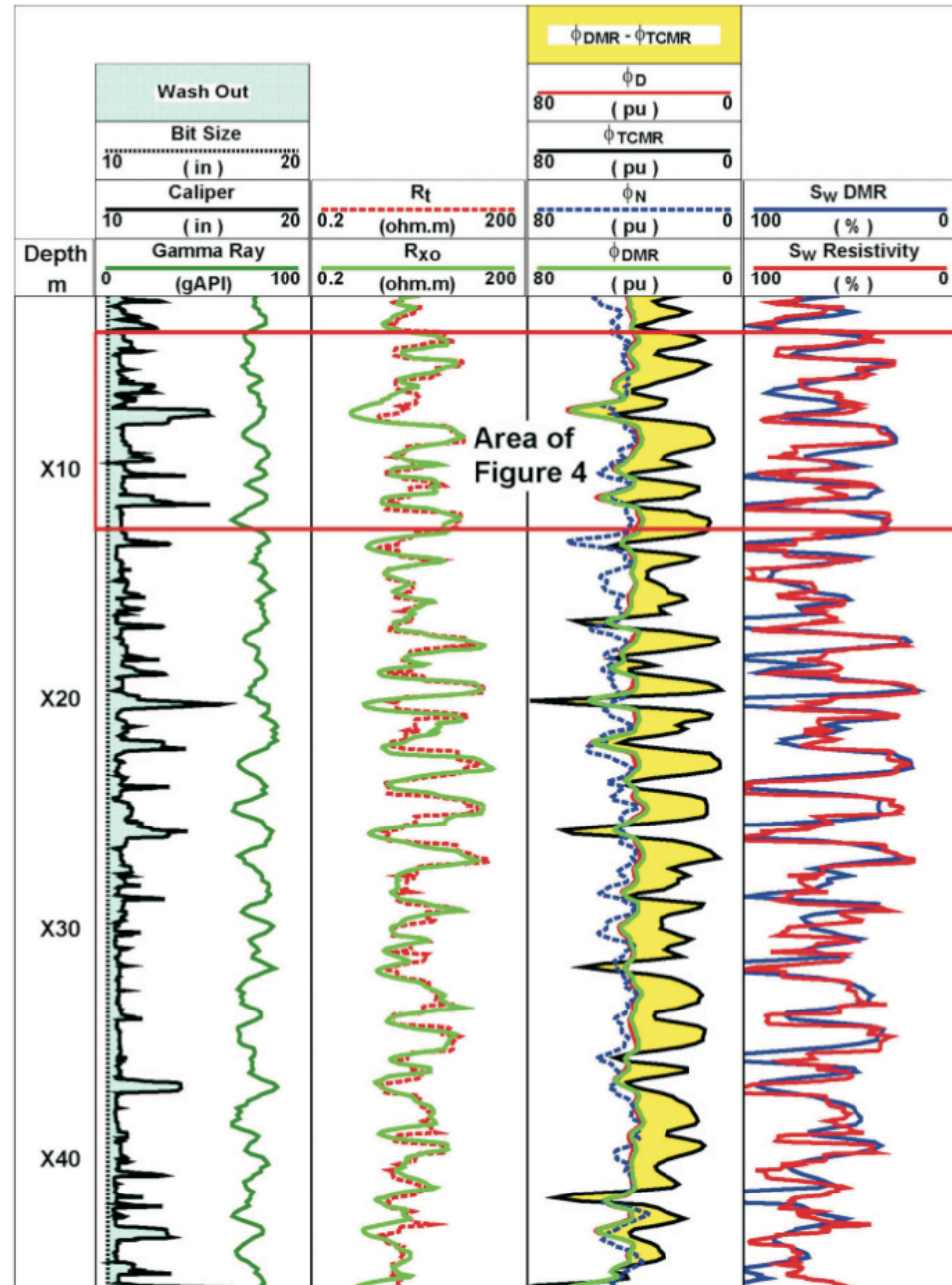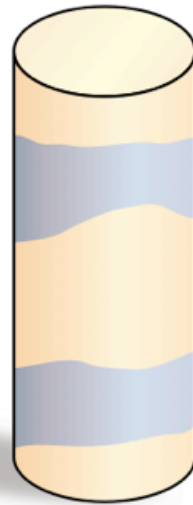
Pore habit of gas hydrates
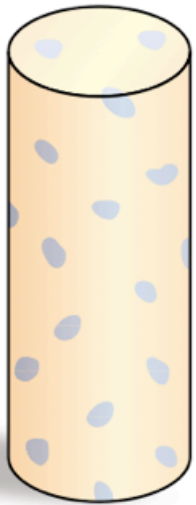
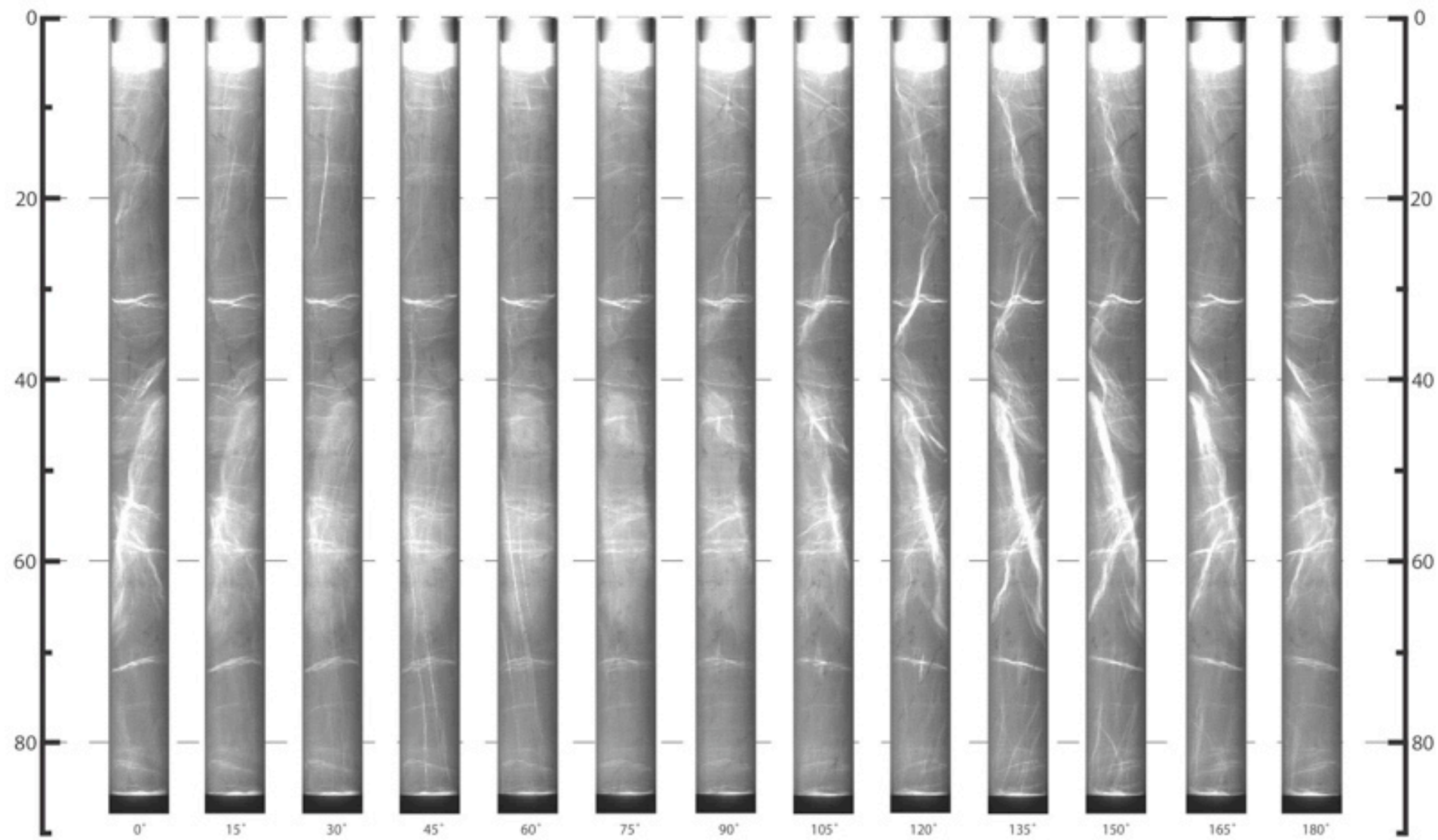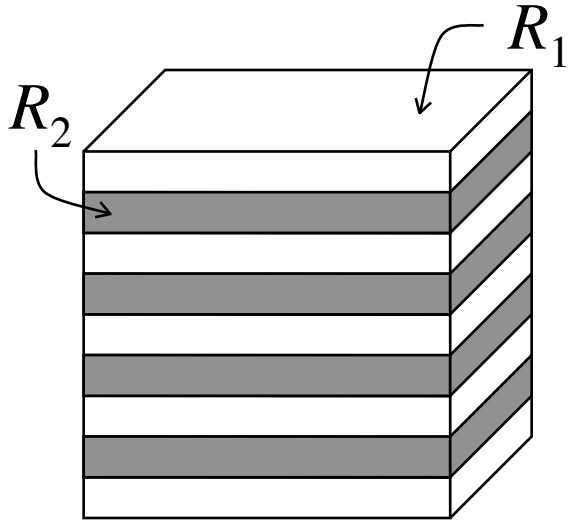Disseminated cement   Nodules   Veins   Massive layers

^ How hydrate is distributed in sediments. A formation can contain *(left to right)* hydrate as disseminated cement, nodules, veins and massive layers.

Collett et al., 2000

NGHP-1 10B-08Y X-Ray Rotations
Core Pressure 150bar

Unit Cube

$R_1 = 1\ \Omega \cdot \mathrm{m}$

$R_2 = 100\ \Omega \cdot \mathrm{m}$

Horizontal current flow
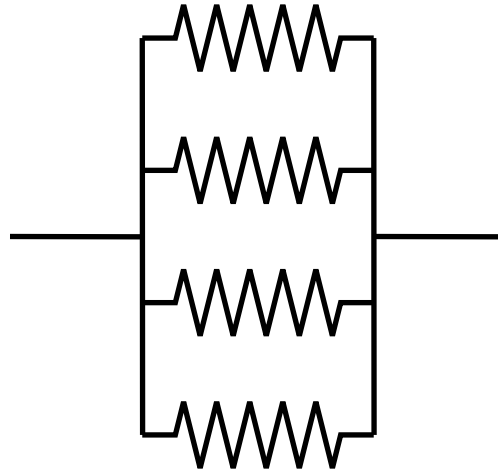
$$R = \left[\frac{1}{2}\left(\frac{1}{R_1} + \frac{1}{R_2}\right)\right]^{-1}$$

$$= \left[\frac{101}{200}\right]^{-1} \approx 2\ \Omega \cdot \mathrm{m}$$

Harmonic mean

Vertical current flow

$$R = \frac{1}{2}(R_1 + R_2)$$

$$= \frac{101}{2} \approx 50\ \Omega \cdot \mathrm{m}$$

Arithmetic mean

Cyclostratigraphy

41 ky sine wave

Magnetic susceptibility

10

5

0

375   380   385   390   395

Core depth (m below sea floor)

Sediment data
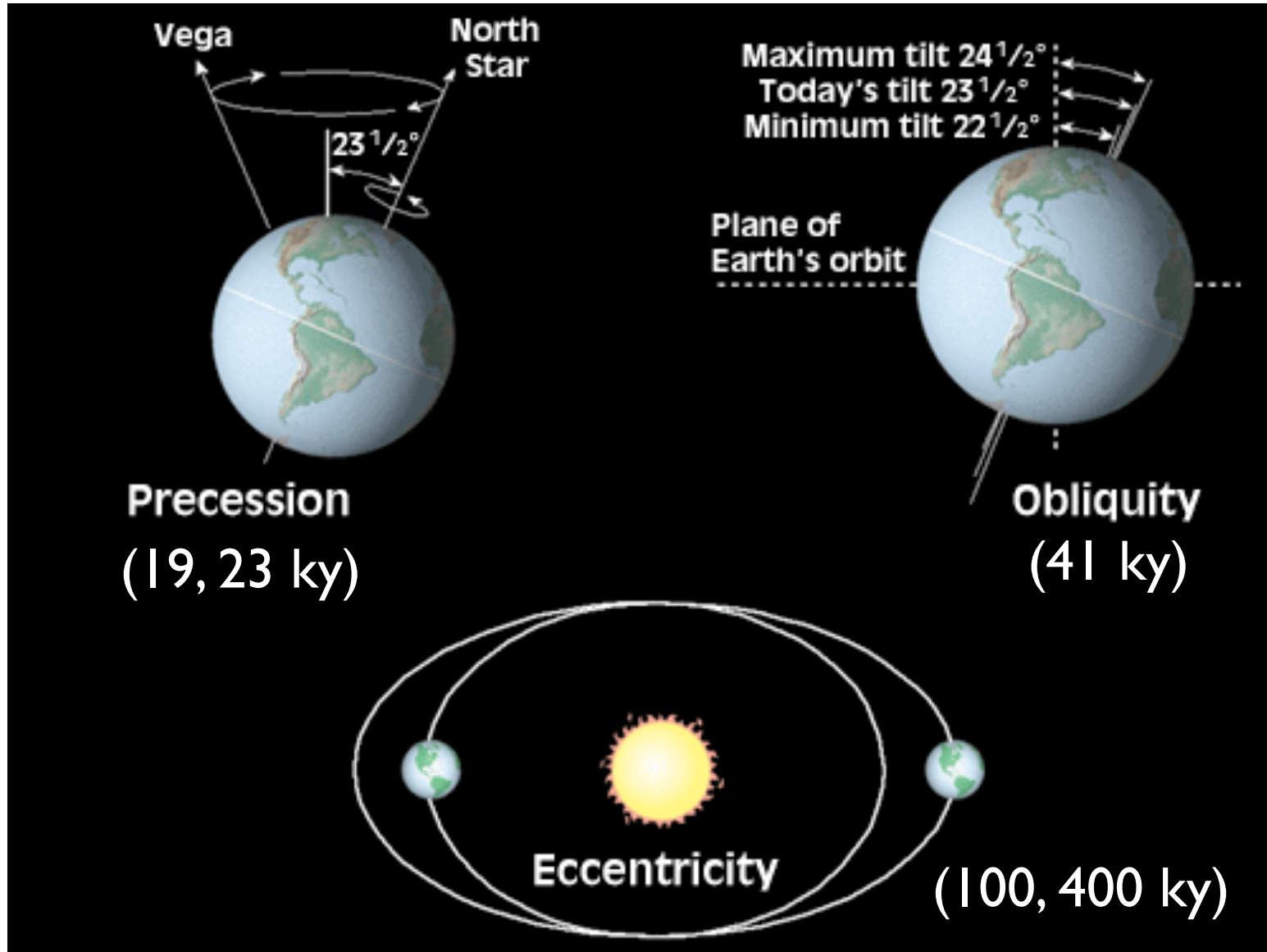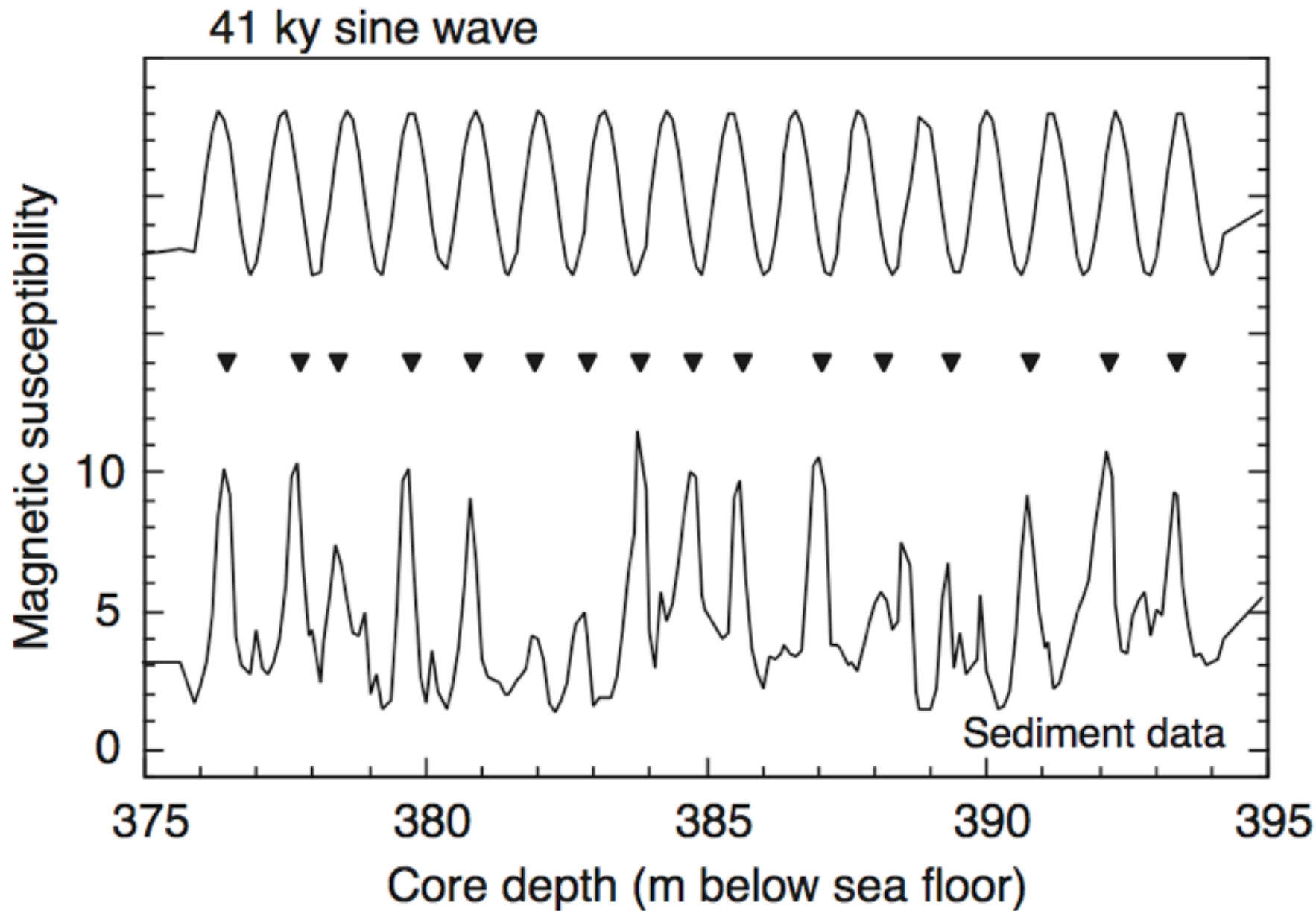
Herbert (2001)

Herbert (2001)

Sedimentation rate drops

Cycle frequency increases

Window for spectral analysis

Frequency (cycles/m)

Stratigraphic depth (arbitrary units)
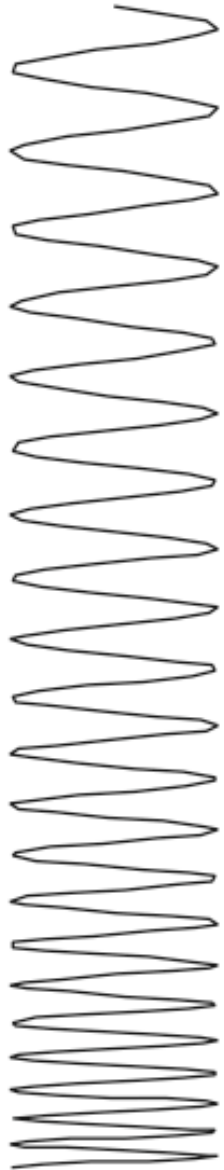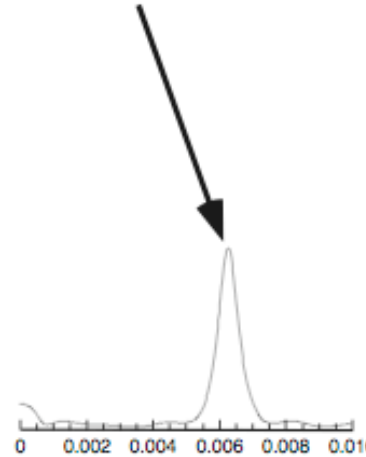
Signal

Fourier spectrum

insolation target

926
SGR

925A

Cenozoic: match insolation target

926C

926B

928B

929A

Age (Ma)

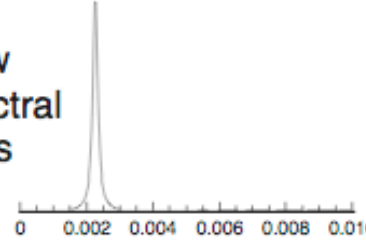Figure 2. Data for the interval 18–22 Ma. Reading from the top: insolation target; downhole spectral gamma ray log for ODP Hole 926B; magnetic susceptibility (volume-normalized SI) for Holes 925A, 926C, 926B, 928B and 929A. Age control points are marked by crosses; peaks in magnetic susceptibility are tied to minima in insolation. Sedimentation rates for Holes 925A, 926B, 928B and 929A and for the 926B downhole log are plotted below the data for these holes (scale m Ma^{-1} on right-hand axis).

Shackleton et al., 1999

Mesozoic and older: match periodicities in "floating" time scales

Fig. 3   a, Detail of carbonate power spectrum, showing peaks at: A, 90 cm (225 kyr); B, 53 cm (108 kyr); C, 48 cm (98 kyr); and D, 36 cm (73 kyr). b, Detail of transmission power spectrum, showing peaks at: E, 171 cm (347 kyr); F, 57 cm (116 kyr); and D (as in a). In a and b, higher-frequency peaks, probably harmonics of the ~100-kyr cycle, are not labelled. c, d, Lower-resolution power spectrum of carbonate (c) and transmission (d) curves plotted as ln variance. 90% confidence interval and bandwidth (vertical and horizontal error bars) calculated following ref. 60.
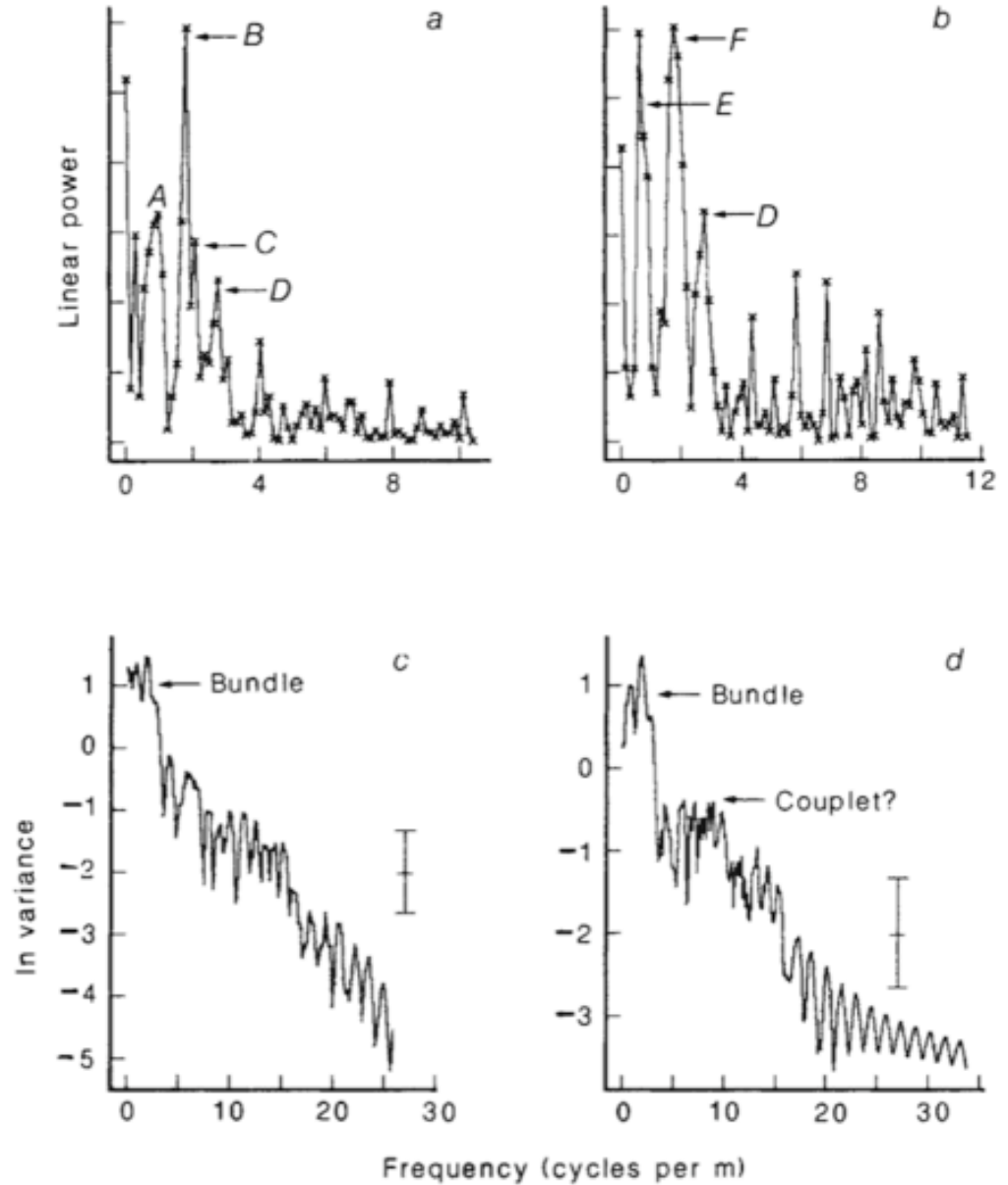
Herbert & Fischer, 1986

Equivalent Time Resolution of Logging Tool Apertures
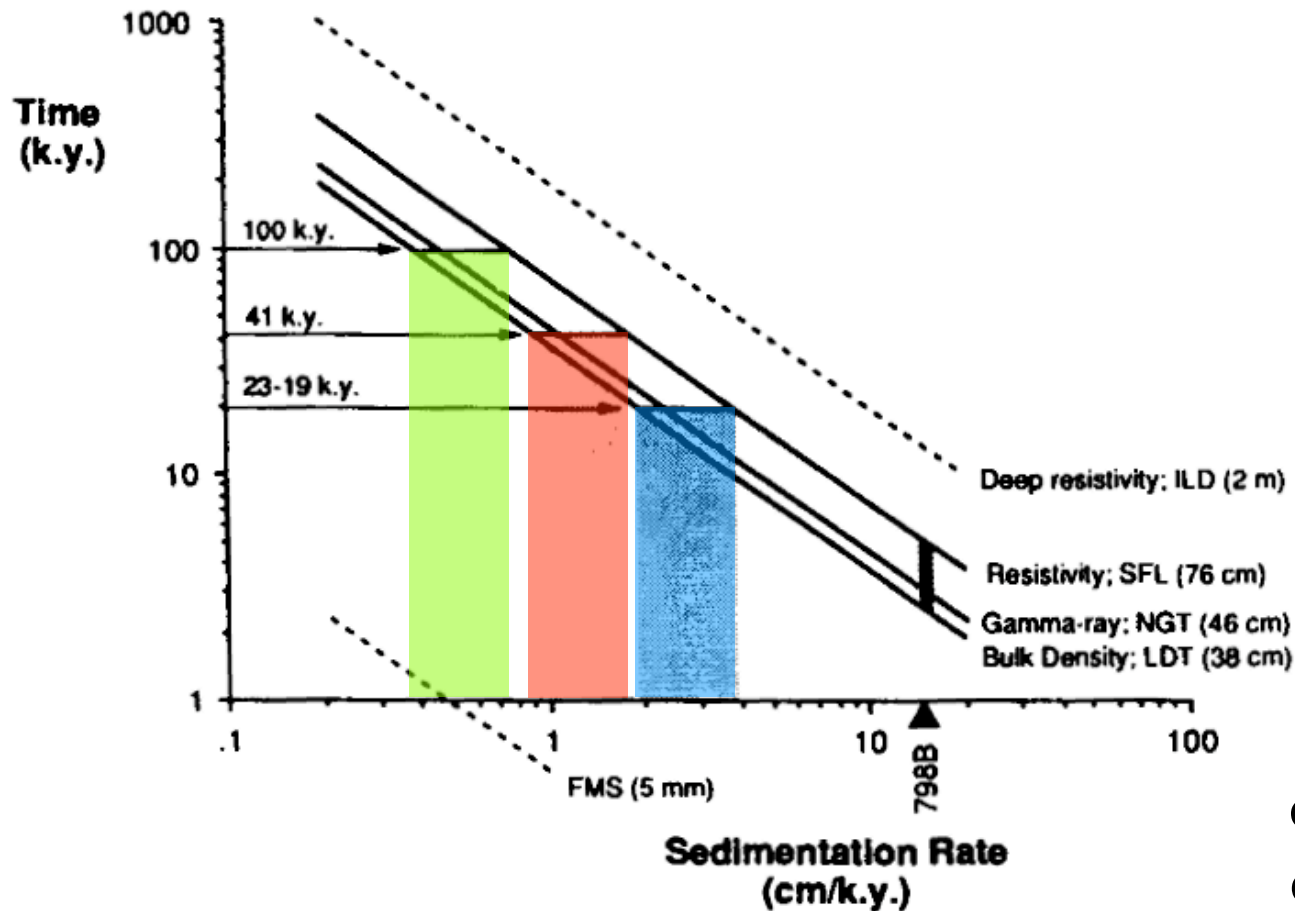
deMenocal et al., 1992

Figure 5. Plot of the temporal resolution of several logging tools as a function of sedimentation rate. Temporal resolution was calculated as vertical aperture/sedimentation rate. Minimum sedimentation rates required to resolve 100 k.y., 41 k.y., and 23–19 k.y. in time are shown as shaded columns. Note that these sedimentation rates are only sufficient to resolve a time interval (Δt) equivalent to 100 k.y., 41 k.y., and 20 k.y.

Hole 798B

deMenocal
et al., 1992
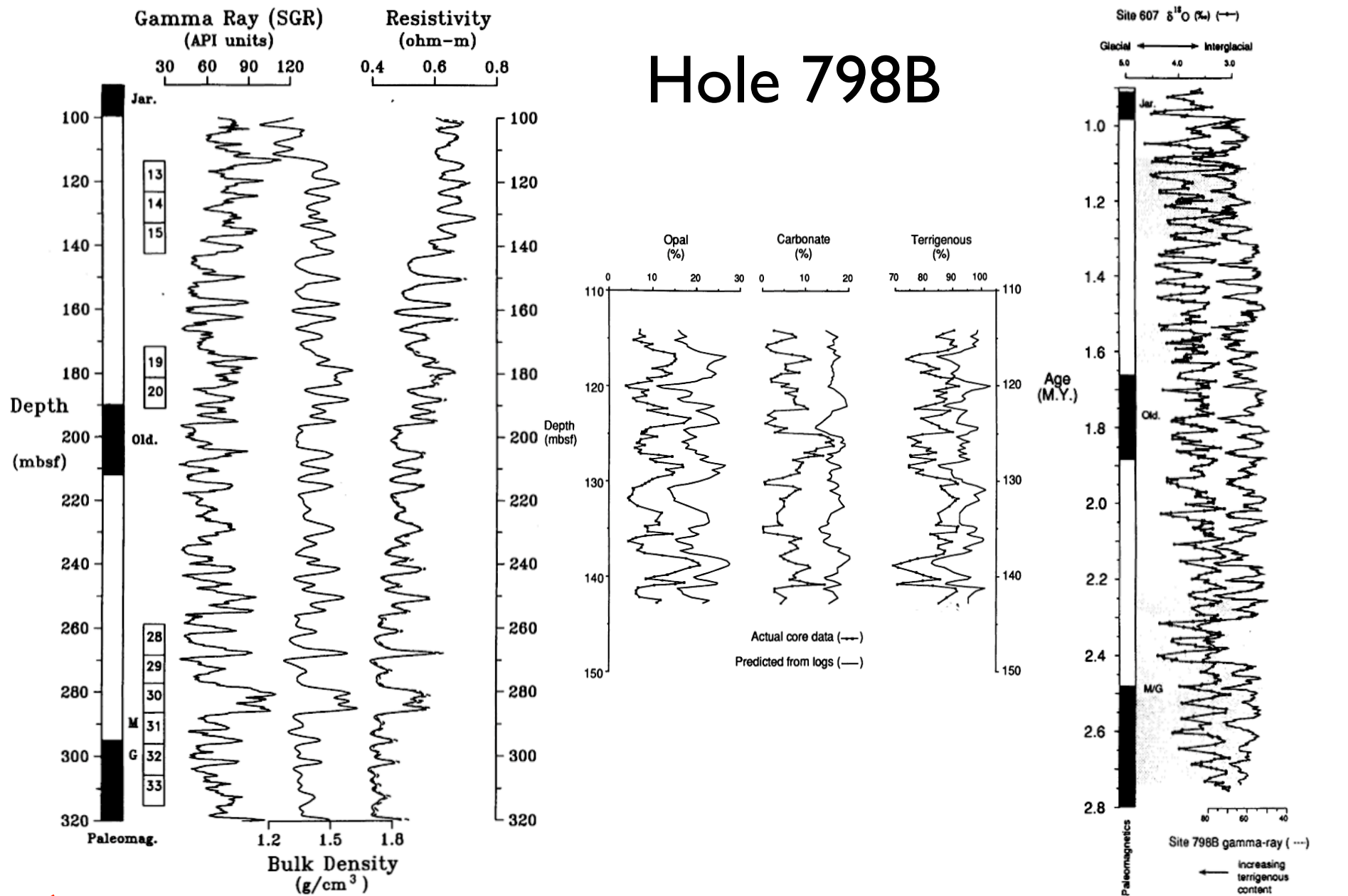
Opal from diatoms
(Glacial)

Terrigenous material
(Interglacial)

Figure 14. Correlation of the Hole 798B SGR gamma-ray log with the marine $\delta^{18}O$ record from Site 607 in the North Atlantic (Raymo et al., 1989; Ruddiman et al., 1989). The SGR time series was initially constrained using the paleomagnetic reversal boundaries. Minor adjustments to the SGR time series were performed using the CORPAC correlation program to improve its alignment with the Site 607 $\delta^{18}O$ record. The age-depth plot resulting from this process is shown in Figure 15.

Formation MicroImager (FMI)

Upper electrode

Mass insulated sub
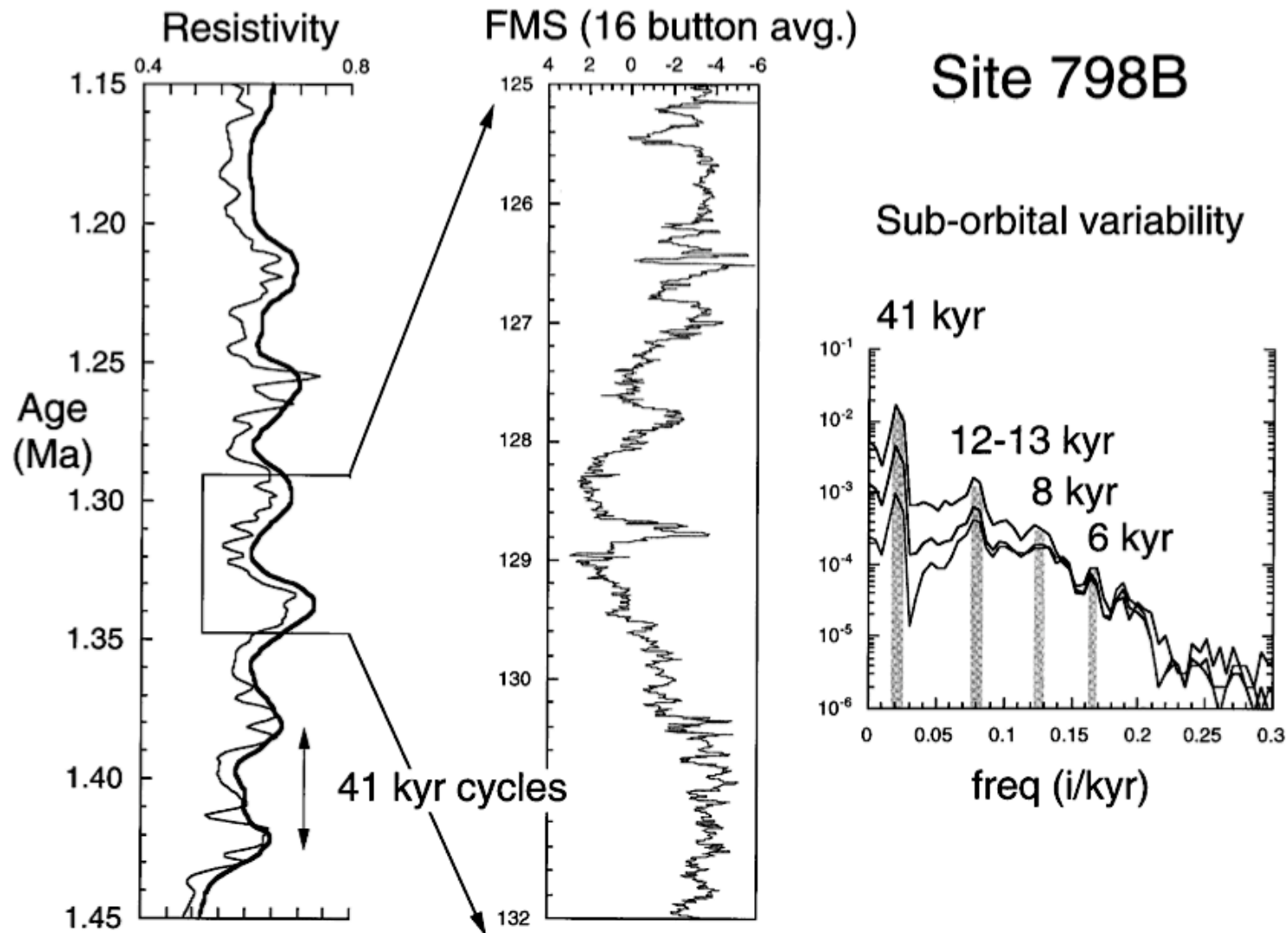
Current

Lower electrodes

5 mm
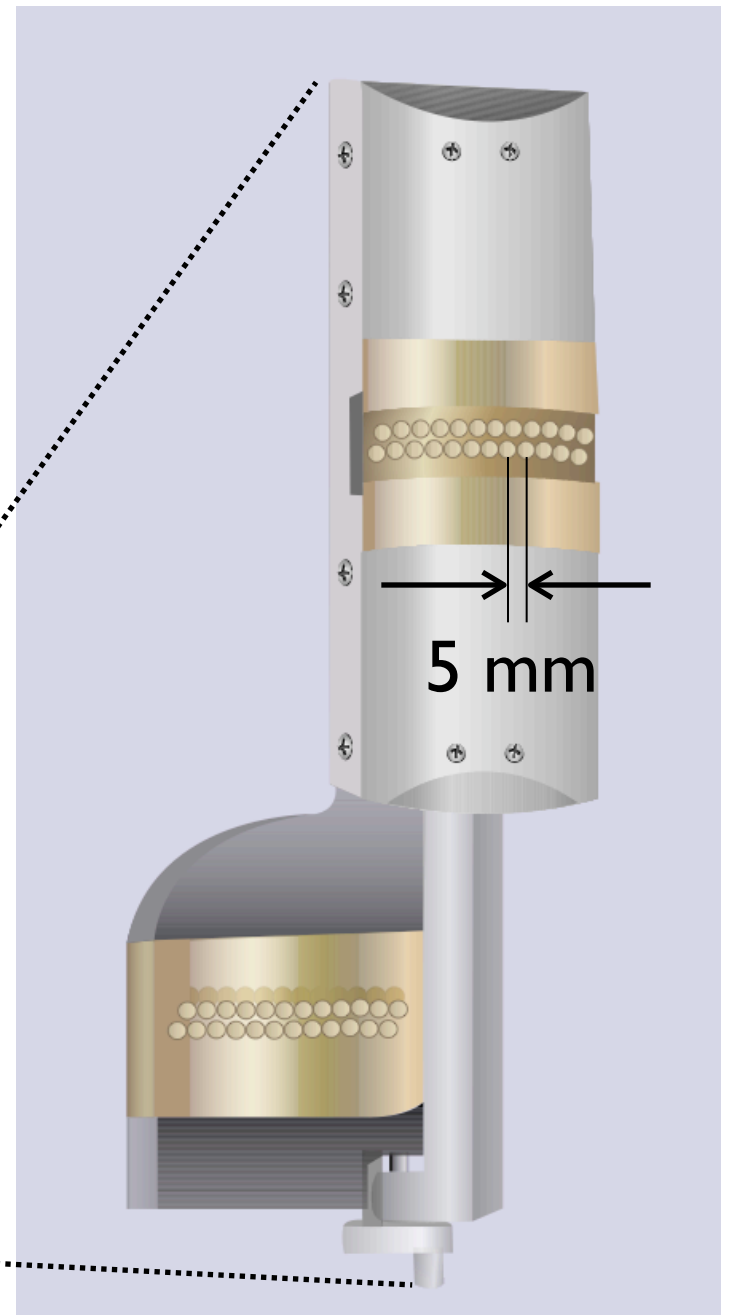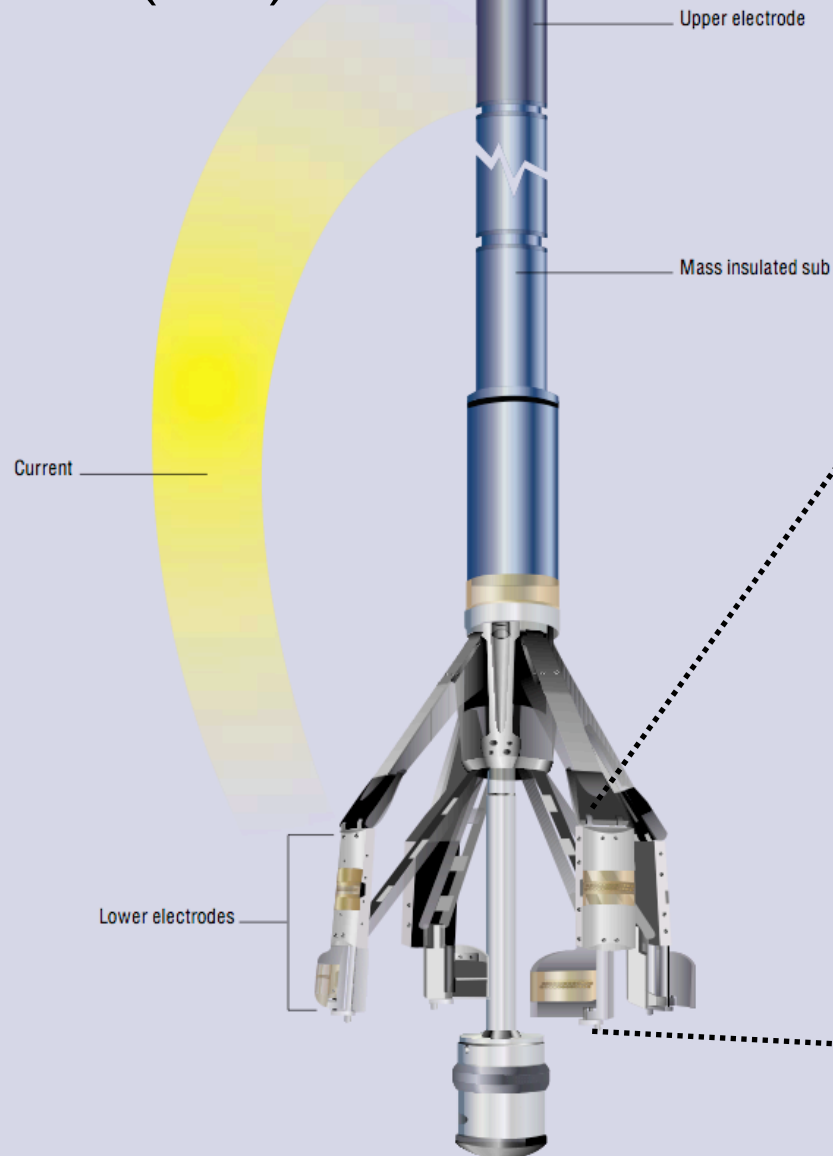
Figure 9. Comparison of data from three wireline resistivity tools: shallow and deep resistivity and the averaged FMS record that show cycles at a 41,000-year orbital period and below in the comparative power spectra [after *deMenocal and King*, 1995]. The resistivity logs have been converted to age, and the averaged FMS data are plotted on relative scale over a 7-m interval. The fine vertical resolution of the FMS data allows observation of periods as short as 6000 years.